iScience

CellPress
OPEN ACCESS

Article

N6-methyladenosine modification promotes hepatocarcinogenesis through circ-CDYL-enriched and EpCAM-positive liver tumor-initiating exosomes

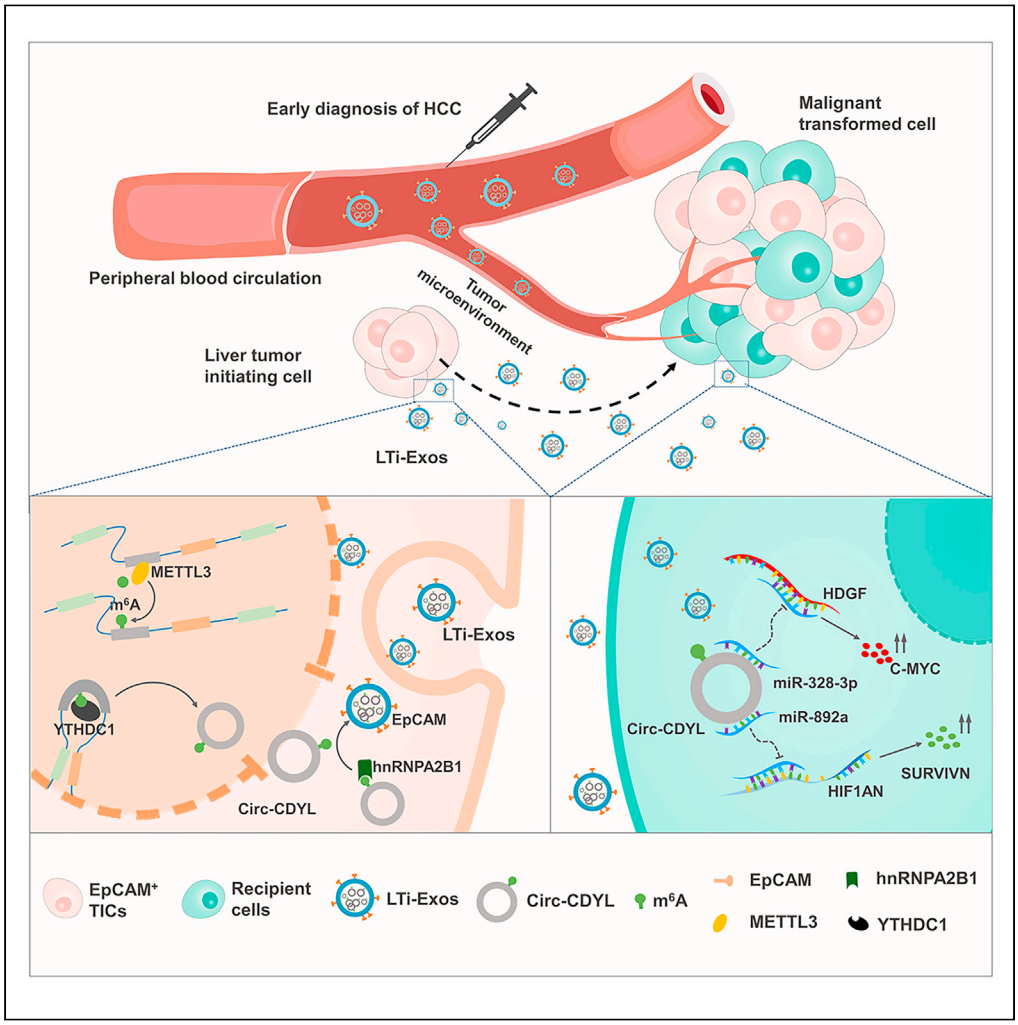

Yanping Wei, Jingbo Fu, Hailing Zhang, ..., Yexiong Tan, Liang Li, Hongyang Wang

yxtan1214@163.com (Y.T.)
liliangyuanquan@163.com (L.L.)
hywangk@vip.sina.com (H.W.)

Highlights

Circ-CDYL is substantially enriched in the plasma exosomes of early HCC patients

Circ-CDYL-enriched and EpCAM-positive exosomes act as liver tumor-initiating exosomes

m6A modification promotes Circ-CDYL biogenesis by promoting back-splicing progress

m6A modification facilitates the sorting of Circ-CDYL into exosomes via hnRNPA2/B1

Wei et al., iScience 26, 108022
October 20, 2023 © 2023
https://doi.org/10.1016/j.isci.2023.108022

iScience

CellPress
OPEN ACCESS

Article

N6-methyladenosine modification promotes hepatocarcinogenesis through circ-CDYL-enriched and EpCAM-positive liver tumor-initiating exosomes

Yanping Wei,[1,2,8] Jingbo Fu,[1,2,8] Hailing Zhang,[3,8] Yan Ling,[4,8] Xuewu Tang,[5,2] Shuowu Liu,[1,2] Miao Yu,[1,2] Fuyan Liu,[1,2] Guokun Zhuang,[1,2] Haihua Qian,[1,2] Kecheng Zhang,[6] Pinhua Yang,[6] Xinwei Yang,[6] Qi Yang,[1,2] Shennian Ge,[1,2] Baohua Zhang,[6] Yexiong Tan,[1,2,*] Liang Li,[1,2,*] and Hongyang Wang[1,2,7,9,*]

SUMMARY

CircRNAs play multiple roles in a variety of cellular processes. We found that Circ-CDYL is highly enriched in early HCC plasma exosomes. Moreover, EpCAM$^+$ HCC cells and exosomes had significant Circ-CDYL levels. We postulated that Circ-CDYL-enriched and EpCAM-positive exosomes would function as liver tumor-initiating exosomes (LTi-Exos). As predicted, intercellular transfer of LTi-Exos activates the HDGF-PI3K-AKT-mTOR and HIF1AN-NOTCH2 axes in recipient cells, promoting malignancy. Upstream, we found that the N6-methyladenosine (m^{6}A) modification of Circ-CDYL exerted its action in HCC cells through a dual mechanism. First, it stimulated back-splicing processes via YTHDC1 to promote Circ-CDYL biogenesis. Second, it facilitates the active sorting of Circ-CDYL into exosomes via hnRNPA2/B1. Clinically, the combination of LTi-Exos and plasma alpha-fetoprotein (AFP) provides a promising early diagnostic biomarker for HCC with an AUC of 0.896. This study highlights the effect and mechanism by which m^{6}A modification promotes hepatocarcinogenesis via modulation of the tumor microenvironment by LTi-Exos.

INTRODUCTION

Hepatocellular carcinoma (HCC) is the second leading cause of cancer-related death worldwide in men, and its rising global prevalence highlights the need for effective strategies that can reduce the burden of tumors.[1] Previous research has shown that neoplasm stage plays a crucial role in determining HCC prognosis: the 5-year survival rate for all-stage HCC patients is disappointingly low at 14% overall.[2] However, the 5-year survival rate for patients with very early stage (Barcelona Clinic Liver Cancer stage 0, BCLC stage 0) and early stage (BCLC stage A) HCC approaches 90% and 50%–70% after active surgical treatment, respectively.[3–5] A subgroup analysis revealed that the optimal median survival time for HCC patients with BCLC stage A is 53 months. The median survival time for patients with BCLC stages B/C/D is only 16, 7, and 3 months, respectively.[6] Due to the significant difference in clinical outcome between patients with HCC at early and late stages, the importance of early screening and diagnosis for HCC high-risk populations has been emphasized. Unfortunately, although accumulating data encourage the early detection of HCC, the lack of specific symptoms in the early HCC,[7] the suboptimal performance of ultrasound examination,[8,9] and the insufficient biomarker AFP for HCC screening[10,11] caused inevitable serious obstacles in the clinic. The inadequacies of currently available methods for HCC screening and early diagnosis necessitate the development of an innovative sufficient surveillance modality in clinical practice.

Exosomes are specialized, nanosized, membrane-bound endocytic vesicles released by various types of cells through inward budding of the limiting membrane of endosomes.[12,13] Abundant cargoes of various DNA, mRNA, lncRNA, microRNA, and circRNA are encapsulated and stabilized in exosomes, which enables them to transmit intracellular cargoes and participate in intercellular communication when they fuse with target cells.[14,15] Exosomes secreted by tumor cells are implicated in the malignant processes of cancer.[15,16] The role of exosomes and their cargos in the diagnosis and progression of cancers such as pancreatic cancer,[17] prostate cancer,[18] and glioblastoma[19] is anticipated to

[1]International Cooperation Laboratory on Signal Transduction, Eastern Hepato-biliary Surgery Institute, Second Military Medical University, Shanghai, China
[2]National Center for Liver Cancer, Shanghai, China
[3]Changhai Hospital, Second Military Medical University, Shanghai, China
[4]Changzheng Hospital, Second Military Medical University, Shanghai, China
[5]Hepato-pancreato-biliary Center, Zhongda Hospital, School of Medicine, Southeast University, Nanjing, China
[6]Department of Biliary Tract Surgery, Eastern Hepatobiliary Surgery Hospital, Second Military Medical University, Shanghai, China
[7]National Laboratory for Oncogenes and Related Genes, Cancer Institute, RenJi Hospital, Shanghai Jiao Tong University, Shanghai, China
[8]These authors contributed equally.
[9]Lead contact
*Correspondence: yxtan1214@163.com (Y.T.), liliangyuanquan@163.com (L.L.), hywangk@vip.sina.com (H.W.)
https://doi.org/10.1016/j.isci.2023.108022

be crucial. However, the roles of liver cancer-derived exosomes in HCC malignancies, as well as the clinical significance of exosomal cargos in the diagnosis and treatment of HCC, are poorly understood.

The recently discovered noncoding RNA called circRNA, which has a structure that is covalently closed and does not have 3′ or 5′ free ends, is frequently expressed in a tissue- or developmental stage-specific manner.[20,21] CircRNAs are unusually stable in biological processes due to their constitutive resistance to exonuclease activity.[22] There is accumulating evidence that exosomes containing circRNA in body fluids have been identified as promising diagnostic cancer biomarkers due to their selective cargo wrapping and similarity to the cells from which they originated.[12,13]

One of the most common and abundant internal modifications in both coding and noncoding transcripts, such as circRNAs, is N6-methyladenosine (m^6A) modification, which is defined as methylated adenosine at the N6 position.[23] Multiple posttranscriptional processes involving circRNAs are affected by m^6A modification, including back-splicing,[24] export,[25] stability,[26] and translation.[27] Importantly, dysregulation of m^6A profiles has been implicated in the carcinogenesis and progression of HCC.[28,29] Although the two-by-two interrelationship between m^6A modification, circRNAs, and HCC has been repeatedly demonstrated, it is not well understood whether m^6A modification can affect the initiation and progression of HCC by modifying circRNAs.

Our previous study clarified the intracellular function of Circ-CDYL, which is specifically elevated in the early HCC.[30] We found that Circ-CDYL promotes HCC through regulating the expression of mRNAs encoding HDGF and HIF1AN by acting as the sponge of miR-892a and miR-328-3p, which enhances the stemness of HCC cells in sequence. However, the origin of aberrant expression of Circ-CDYL, and whether Circ-CDYL exerts intercellular function in early HCC remain unknown. This study demonstrates that plasma exosomes from patients with early HCC (BCLC stage 0 or A HCC) are enriched for Circ-CDYL, the circRNA that is most significantly increased at this stage. Intriguingly, more EpCAM-positive cells and exosomes were produced by HCC cells in which Circ-CDYL was overexpressed. Moreover, Circ-CDYL expression was higher in both $EpCAM^+$ HCC cells and exosomes. Our working hypothesis was that this subpopulation of liver tumor-initiating exosomes (LTi-Exos) enriched in Circ-CDYL and EpCAM would initiate tumor growth in the liver via the microenvironment. Consequently, circulating LTi-Exos may serve as an ideal marker for the early diagnosis of HCC. Upstream, Circ-CDYL m^6A RNA modification stimulated back-splicing via YTHDC1 to promote Circ-CDYL biogenesis in HCC cells and sorting Circ-CDYL into LTi-Exos via hnRNPA2/B1. STM2457 inhibition of the m^6A writer METTL3 or Circ-CDYL methylation modification sites mutation inhibited the hepatocarcinogenic effect of LTi-Exos. Our data thus provide evidence that LTi-Exos may serve as a potential early screening biomarker and therapeutic target for HCC.

RESULTS

Circ-CDYL is enriched in exosomes from early HCC patients and in $EpCAM^+$ exosomes secreted from HCC cells

Targeting very early-stage HCC directly enables the precise identification of early diagnostic biomarkers and therapeutic targets. Our previous microarray assay analyzed the differentially expressed circRNAs across the genome in BCLC stage 0 HCC tissues and nontumorous adjacent tissues and determined that Circ-CDYL is the circRNA with the greatest increase. Annotation of the circRNA probe revealed that Circ-CDYL originated from the head-to-tail splicing of exon 2 of its parental gene, chromodomain Y-like (CDYL), a member of the Y chromosome gene family that is specific to primates.[30]

To learn more about the Circ-CDYL secretion pattern, we next examined exosomes derived from the plasma of HCC patients at various stages. Increased expression of Circ-CDYL was detected in exosomes isolated from BCLC stage 0 and A HCC patients compared with those isolated from healthy controls (Figure 1A). Contrary to expectations, patients with BCLC stages B and C HCC did not exhibit significantly elevated exosomal Circ-CDYL levels, which may have been due to the altered gene profile in each tumor stage.

To explore the origin of plasma-derived exosomal Circ-CDYL, a stable Circ-CDYL-overexpressing cell line and a knockdown cell line were constructed with a lentivirus system using SMMC-7721 and HCCLM3 cells, respectively, based on the relative background expression of Circ-CDYL (Figure 1B). We then purified exosomes from the culture medium of the constructed HCC cell line using ultracentrifugation. Purified exosome samples exhibited similar sizes (diameters ranging from 20 to 200 nm) (Figure S1A) and typical cup-shaped morphology (Figure S1B). Furthermore, the identity of exosomes was confirmed by the positive exosomal protein markers TSG101, HSP70 and CD63 and the negative marker Calnexin (Figure S1C). Consistent with the expression pattern in parental cells (Figure 1B), the Circ-CDYL level was significantly higher in exosomes released from SMMC-7721 cells stably overexpressing Circ-CDYL (Figure 1C). Inhibition of Circ-CDYL expression in HCCLM3 cells led to the opposite effects (Figure 1C). These results indicated that the high exosomal Circ-CDYL originated from HCC cells with increased expression of Circ-CDYL.

Stem-like cells such as tumor-initiating cells (T-ICs) within tumors are a unique subpopulation of cells responsible for the initiation and progression of cancer. Liver T-ICs are characterized by several cell marker molecules, such as epithelial cell adhesion molecule (EpCAM), PROM1 (CD133) and CD24.[31–33] We further examined whether Circ-CDYL, which is markedly highly expressed in very early-stage HCC, could affect the characteristics of liver T-ICs. HCC cells collected from nonattached spheroids, where T-ICs are enriched,[18] showed higher expression of Circ-CDYL (Figure S2A). To further explore which subpopulation of T-ICs was associated with Circ-CDYL, we detected the proportion of T-ICs with liver stem-like cell markers in constructed HCC cell lines using flow cytometry assays. We observed that overexpression of Circ-CDYL especially elevated the proportion of $EpCAM^+$ (Figure 1D) but not $CD133^+$ and $CD24^+$ liver T-ICs (Figures S2B and S2C). As a result, the proportion of $EpCAM^+$ cells decreased when Circ-CDYL expression was inhibited in HCCLM3 cells (Figures 1D, S2B, and S2C). Consistently, ectopic overexpression of Circ-CDYL resulted in higher protein levels of EpCAM in HCC cells, while knockdown of Circ-CDYL showed the opposite effect. The exosomal level of EpCAM was synchronized with that of intracellular EpCAM (Figure 1E). This trend was similar to the expression pattern of exosomal Circ-CDYL synchronized with intracellular Circ-CDYL (Figures 1B and 1C).

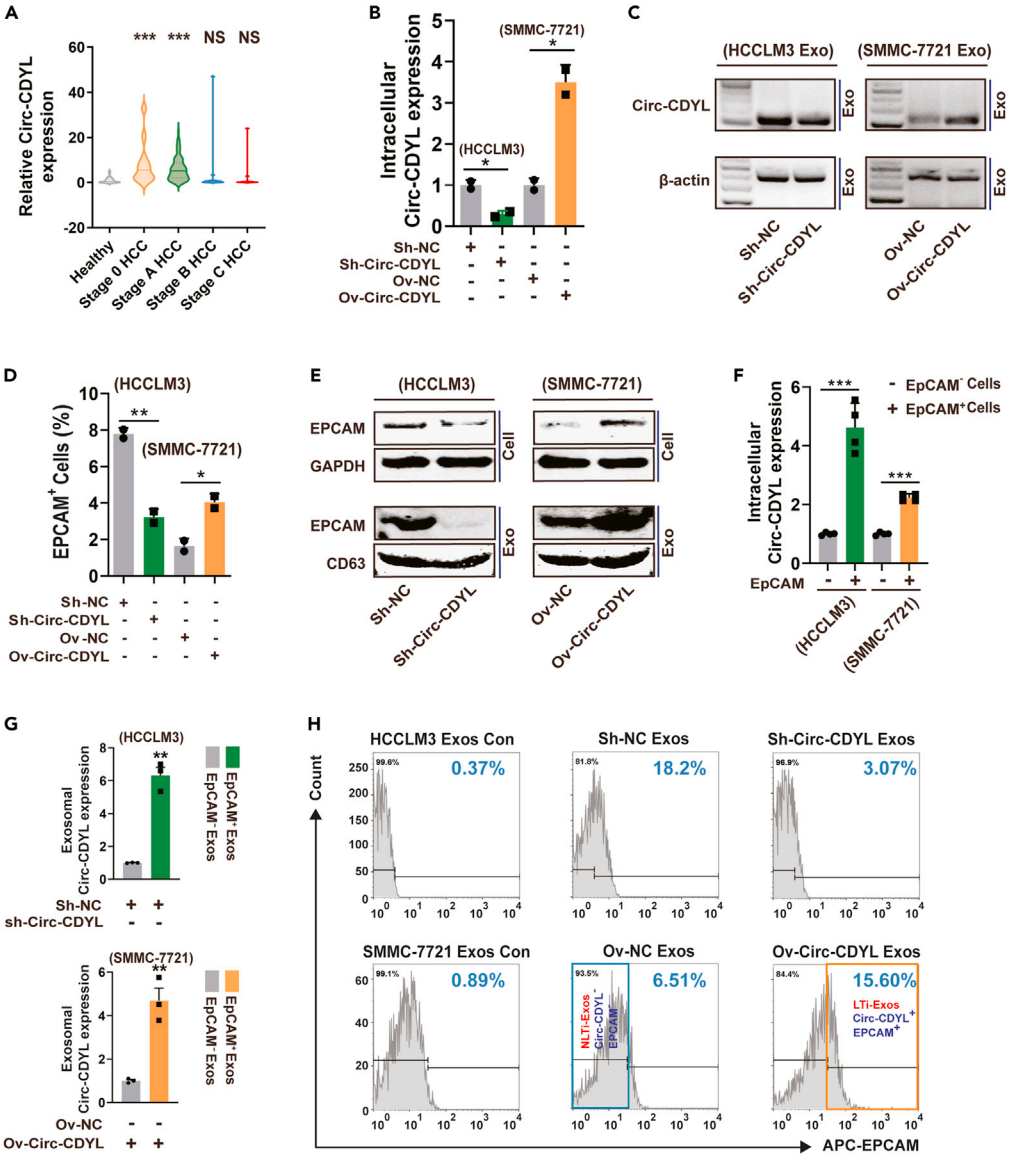

Figure 1. Circ-CDYL and EpCAM share close connections in HCC cells and exosomes

(A) The expression of Circ-CDYL was determined in exosomes isolated from the plasma of different stages of HCC patients (n = 24, 71, 21, and 20 for BCLC stage 0, A, B, C HCC, respectively) and 46 healthy donors.

(B) RNA expression level of Circ-CDYL determined by RT−qPCR and depicted by relative quantity calculation using the $2^{-\Delta\Delta CT}$ value. Stable Circ-CDYL knockdown HCCLM3 cells and Circ-CDYL-overexpressing SMMC-7721 cells were constructed by a lentivirus system.

(C) RNA expression of Circ-CDYL in exosomes isolated from the cell culture supernatant of Circ-CDYL knockdown and Circ-CDYL-overexpressing HCC cells, as determined using RT−PCR followed by agarose gel electrophoresis.

(D) The percentage of EpCAM-positive ($EpCAM^+$) cells determined by flow cytometry in Circ-CDYL-knockdown and Circ-CDYL-overexpressing HCC cells.

(E) Protein levels of EpCAM in the indicated cells and corresponding cell-derived exosomes.

(F) Circ-CDYL expression was determined in flow cytometry-sorted primary $EpCAM^+$ and $EpCAM^-$ HCC cells using RT−qPCR.

(G) Circ-CDYL expression was determined in flow cytometry-sorted primary $EpCAM^+$ and $EpCAM^-$ exosomes purified from the cell culture supernatant of the indicated HCC cells.

(H) Flow cytometry analysis showed the percentage of $EpCAM^+$ exosomes released from Circ-CDYL-ectopically expressed HCC cells. Exos, exosomes; Con, negative control using isotype antibody of anti-EpCAM; LTi, liver tumor-initiating; NLTi, nonliver tumor-initiating.

To ascertain the relationship between Circ-CDYL and EpCAM, we further explored the correlation between the expression of these two molecules at both cellular and exosomal scales. Statistically, we found that the intracellular expression level of Circ-CDYL was higher in $EpCAM^+$ HCC cells than in $EpCAM^-$ cells (Figure 1F). The exosomal level of Circ-CDYL in sorted $EpCAM^+$ exosomes was higher than that

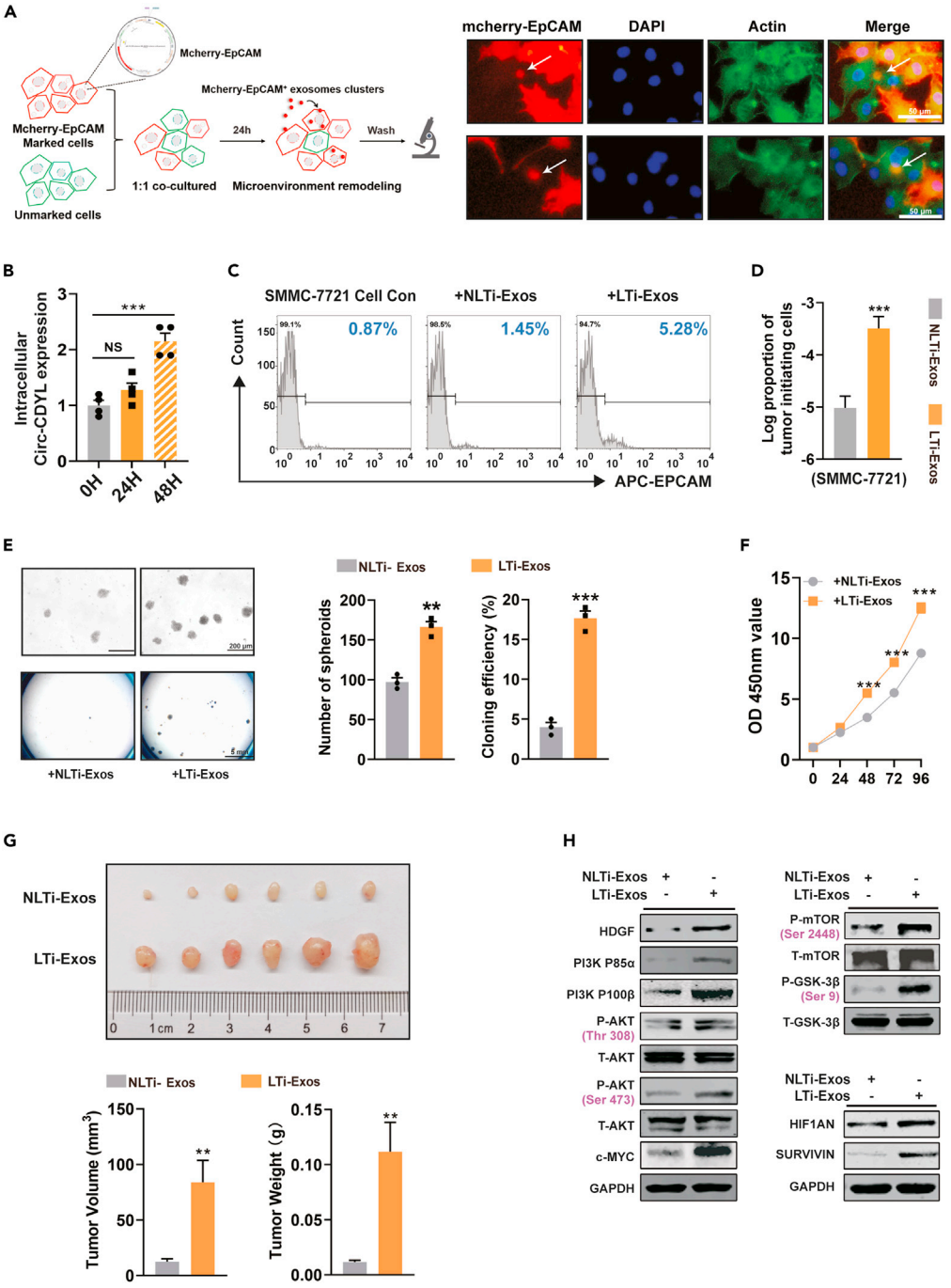

Figure 2. LTi-Exos boosted hepatocarcinogenesis via the tumor microenvironment by performing functions similar to tumor-initiating cells

(A) Diagram of LTi-Exos uptake. SMMC-7721 cells stably expressing mCherry-EpCAM fusion protein (marked cells, red) were cocultured with negative control cells (unmarked cells) at a ratio of 1:1. After 24 h, the cell supernatant was removed, and all cells were dyed with actin-tracker probe (green) and DAPI (blue). White arrows indicate EpCAM$^+$ exosome cluster uptake by HCC cells.

(B) The expression levels of Circ-CDYL in SMMC-7721 cells after incubation with LTi-Exos for 24 h and 48 h were determined.

(C) The percentage of EpCAM$^+$ cells was determined by flow cytometry analysis 48 h after treatment with LTi-Exos or NLTi-Exos. Con, negative control using an isotype antibody against EpCAM.

(D) The proportion of T-ICs in SMMC-7721 cells was assessed by limiting dilution assay after incubation with LTi-Exos or NLTi-Exos for 48 h.

(E) Determination of spheroid formation in low-adhesion plates (upper). Colony formation was evaluated (below).

(F) SMMC-7721 cell proliferation was evaluated by CCK8 assay at different time points after incubation with LTi-Exos or NLTi-Exos.

Figure 2. *Continued*

(G) After incubation with LTi-Exos or NLTi-Exos for 48 h, 5×10^5 SMMC-7721 cells were subcutaneously injected into male nude mice (n = 6). The tumors were harvested, and their volume and weight were measured at 3 weeks after injection.

(H) Western blot showing the expression levels of HDGF, P85α/P110β regulatory subunit of PI3K, phosphorylation of AKT and mTOR, c-MYC, HIF1AN, and SURVIVIN.

in $EpCAM^-$ exosomes (Figure 1G). Circ-CDYL-overexpressing SMMC-7721 cells produced a significantly higher proportion of $EpCAM^+$ exosomes (15.60% vs. 6.51%, Figure 1H). Conversely, interference with Circ-CDYL expression in HCCLM3 cells led to a significantly decreased proportion of $EpCAM^+$ exosomes (18.20% vs. 3.07%, Figure 1H). In addition, when flow cytometry analysis was executed, we found that the proportion of $EpCAM^+$ exosomes was markedly higher than the proportion of $EpCAM^+$ parent cells. In SMMC-7721 cells and HCCLM3 cells, $EpCAM^+$ cells accounted for a mean of 1.64% and 7.78%, respectively (Figure 1D). However, in SMMC-7721-secreted exosomes and HCCLM3-secreted exosomes, $EpCAM^+$ exosomes accounted for 6.51% and 18.2%, respectively (Figure 1H). This result indicated that EpCAM has an enriching effect in the exosomes secreted by HCC cells.

Based on these results, it is reasonable to assume that Circ-CDYL and EpCAM are very closely related at both the HCC cell and exosome scales, and both may together constitute a specific HCC cell or exosome subtype. Because $EpCAM^+$ liver cells are defined as liver tumor-initiating cells,[32] we postulated that this subpopulation of Circ-CDYL-rich and $EpCAM^+$ exosomes will work as liver tumor-initiating exosomes (LTi-Exos, orange frame, Figure 1H). Accordingly, another subpopulation of $EpCAM^-$ exosomes with low levels of Circ-CDYL could be regarded as non-liver tumor initiating exosomes (NLTi-Exos, Blue Frame, Figure 1H).

LTi-Exos promote early hepatocarcinogenesis through the tumor microenvironment

Exosomes perform their functions by delivering biomolecules, including lipids, proteins, and RNAs, to recipient cells.[34] To investigate the effects and functions of LTi-Exos-mediated intercellular communication, we utilized PKH26 to label the sorted LTi-Exos (orange frame, Figure 1H) and then incubated them with SMMC-7721 recipient cells. The recipient cells, as anticipated, took up the PKH26-labeled LTi-Exos in the culture supernatant (Figure S3A). To further simulate the process of natural formation and intercellular communication of LTi-Exos, HCC cells stably expressing mCherry-EpCAM fusion protein (red) were cocultured with recipient cells (green). After the cell culture supernatant was removed, we observed that EpCAM-positive exosome clusters were absorbed by recipient cells (Figure 2A).

Next, we functionally verified whether LTi-Exos can play a role in tumor initiation. After incubation, recipient HCC cells showed elevated expression of Circ-CDYL (Figure 2B), indicating that the oncogenic Circ-CDYL cargo was delivered into the recipient cell by exosomes. After 48 h of LTi-Exos treatment, more recipient HCC cells were transformed into $EpCAM^+$ T-ICs than NLTi-Exos-treated cells (Figure 2C). In addition, the proportion of tumor-initiating cells estimated by limiting dilution assay increased (Figures 2D and S3B). LTi-Exos also significantly promoted spheroid formation (Figure 2E, upper), colony formation (Figure 2E, lower), and *in vitro* and *in vivo* cell proliferation (Figures 2F and 2G) of recipient cells.

Mechanistically, we verified whether LTi-Exos can cause the activation of Circ-CDYL-driven signal transduction pathways in recipient cells.[30] We found that LTi-Exos elevated HDGF expression, activated the PI3K P85 and P110 subunits and enhanced AKT phosphorylation at the Thr308 and Ser473 sites in sequence, which stimulated the downstream targets mTORC1, GSK-3β and C-MYC more efficiently than NLTi-Exos (Figures 2H and S2D). Similarly, LTi-Exos increased the expression of HIF1AN and SURVIVIN more than NLTi-Exos (Figures 2H and S2D).

Overall, LTi-Exos performed functions similar to those of tumor-initiating cells to significantly promote early hepatocarcinogenesis through the tumor microenvironment.

m^6A modification of Circ-CDYL regulates the stem-like properties of HCC cells

The most common RNA base modification, m^6A modification, may be essential for circRNA biogenesis and function. The consensus motif "RRm6ACH" (R = G or A; H = A, C or U) is favored for the alterations.[35] To explore whether the aberrantly expressed Circ-CDYL in early HCC is also subject to m^6A modification, we first performed bioinformatic prediction. Several "very high confidence" potential m^6A modification sites were found in Circ-CDYL using the SRAMP (http://www.cuilab.cn/sramp/) analysis tools. Using a systematic analysis, six sites with the most potential were chosen for further study (combined score >0.70). (Figures S4A and S4B). Furthermore, m^6A RNA immunoprecipitation (MeRIP) assays validated the m^6A enrichment in the Circ-CDYL sequence (Figure 3A).

m^6A modification is installed by a multicomponent methyltransferase complex (MTC), which is composed of core component methyltransferase-like 3 (METTL3) and methyltransferase-like 14 (METTL14) heterodimers.[23] A previous study showed that METTL3 regulates the expression of RNA in a m^6A-dependent manner.[36] To explore the function of m^6A modification in Circ-CDYL, a stable METTL3-overexpressing HCC cell line was constructed with a lentivirus system using SMMC-7721 cells (Ov-METTL3) (Figure S5A). Overexpression of METTL3 significantly increased the level of m^6A modification in Circ-CDYL (Figure 3B). Ligase-dependent absolute quantification analysis (Figure S5B) was presented for quantifying the m^6A ratio at the 6 predicted modified loci with "very high confidence" from extracted total RNA (Figure 3C). The methylation fractions of the endogenous specific sites were determined to range from 20.18% to 95.38% in the HCC cell line, among which over 90% of the Circ-CDYL transcript was m^6A-modified at sites 371 and 433, and approximately 75% of Circ-CDYL was modified at site 116 in HCC cells (Figure 3C).

We next investigated the effects of m^6A modification on Circ-CDYL and found that the expression of Circ-CDYL was remarkably elevated by METTL3 (Figure 3D). In contrast, inhibiting METTL3 with STM2457, a selective and orally active METTL3 inhibitor, decreased the

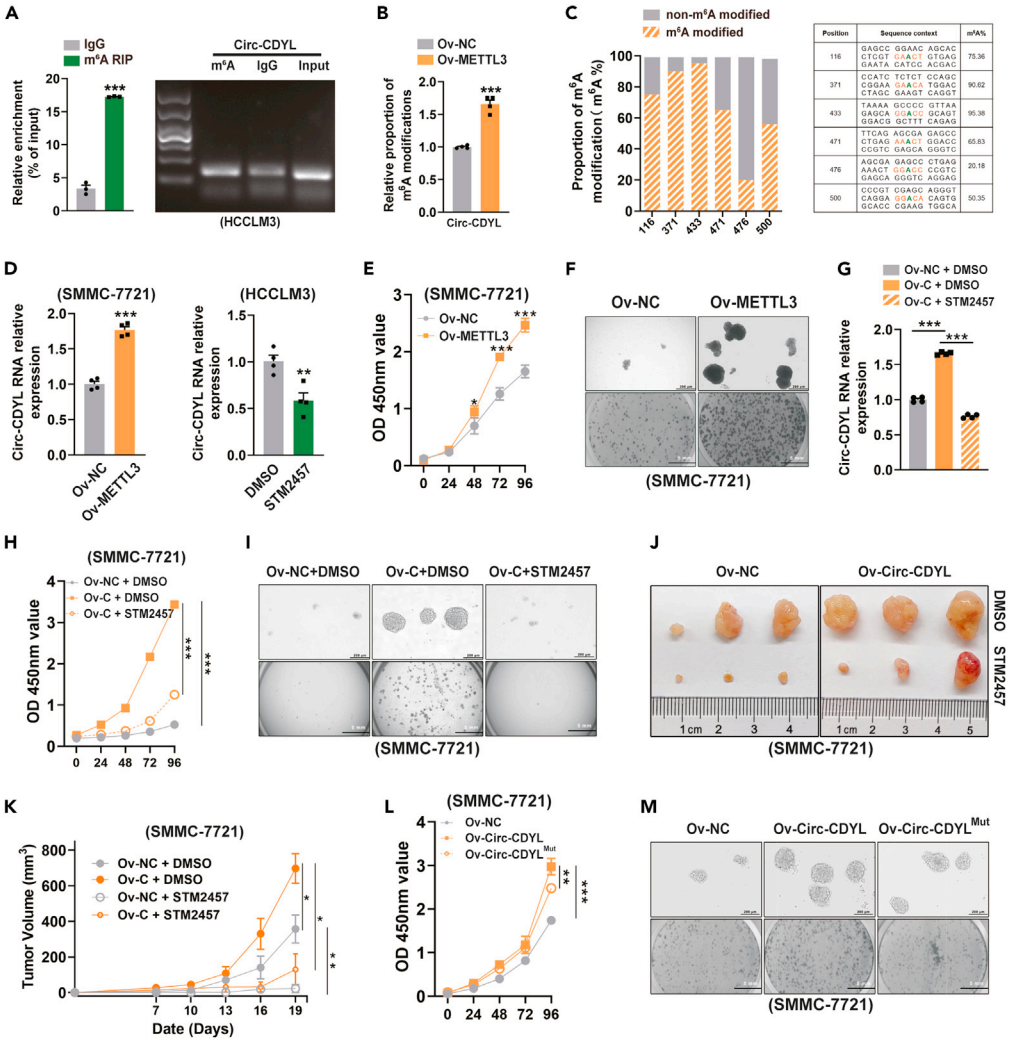

Figure 3. m^{6}A modification of Circ-CDYL by METTL3 aided in HCC tumorigenesis

(A) MeRIP assay followed by RT–qPCR showed an enrichment of Circ-CDYL using an anti-m^{6}A antibody.

(B) The relative proportion of m^{6}A-modified Circ-CDYL was determined using the MazF-qPCR assay in METTL3-overexpressing SMMC-7721 cells and negative control cells.

(C) Ligase-dependent absolute quantification of m^{6}A modification at the predicted "very high confidence" m^{6}A-modified sites in Circ-CDYL.

(D) Relative Circ-CDYL expression was determined in METTL3-overexpressing cells (left) and 48-h STM2457 (5 μM)/DMSO (1:1000 v/v)-treated cells (right) using RT–qPCR.

(E) Cell proliferation was determined in the indicated HCC cells using a CCK-8 assay.

(F) Spheroid formation (upper) and colony formation (below) of the indicated HCC cells.

(G) Relative Circ-CDYL expression was determined in HCC cells after the indicated treatment.

(H and I) Cell proliferation (H), spheroid formation (I, upper) and colony formation (I, below) of HCC cells with the indicated treatment.

(J and K) Tumors were collected from day 19 post tumor implantation in nude mice that had been treated with either STM2457 (50 mg/kg) or vehicle (J). Growth curve of tumor were shown (K).

(L and M) Cell proliferation (L), spheroid formation (M, upper) and colony formation (M, below) of indicated HCC cell lines.

endogenous expression of Circ-CDYL in HCC cells (Figure 3D). These results indicated that the expression of Circ-CDYL could be positively regulated by METTL3 in a m^{6}A-dependent manner.

As ectopic overexpression of Circ-CDYL enhanced the stem-like properties of HCC cells,[30] we next investigated whether METTL3-mediated upregulation of Circ-CDYL has a similar effect. We found that overexpression of METTL3 significantly promoted malignant cell proliferation, spheroid growth and colony formation of HCC cells *in vitro* (Figures 3E–3F and S6A). Furthermore, the elevated level of Circ-CDYL generated by ectopic overexpression could also be reversed by STM2457 (Figure 3G). As anticipated, STM2457 significantly inhibited the increased malignant proliferation, self-renewal, and colony formation ability of HCC cells driven by ectopic overexpression of Circ-CDYL

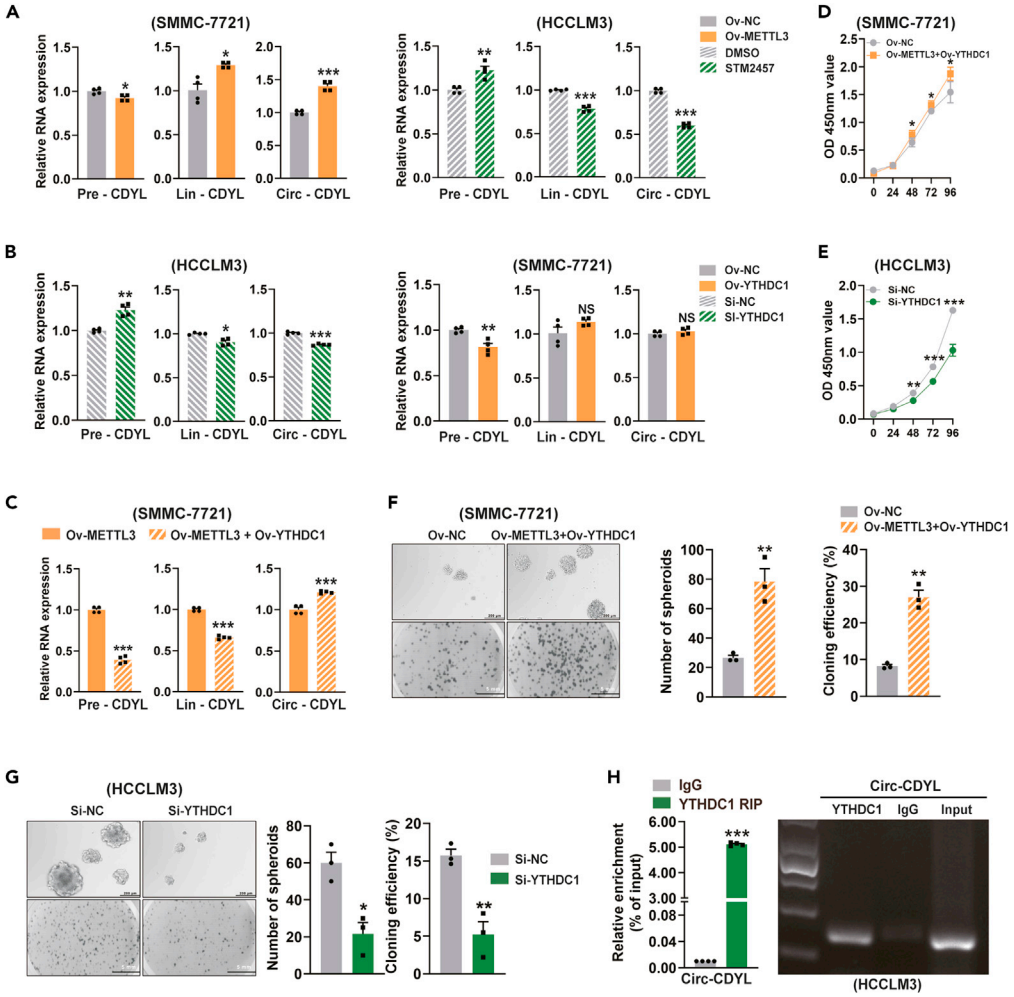

Figure 4. Circ-CDYL back-splicing reaction regulated by METTL3 and YTHDC1-dependent m^{6}A modification

(A–C) Relative RNA levels of the circular transcript (Circ-CDYL), linear transcript (Lin-CDYL), and precursor (Pre-CDYL) in METTL3-disturbed HCC cells (METTL3 overexpression or inhibited by STM2457, respectively) (A), YTHDC1 overexpression (Ov-YTHDC1) or interference cells (Si-YTHDC1) (B), and METTL3 overexpression only or combined overexpression of METTL3 and YTHDC1 cells (C). Values were normalized against β-actin and expressed as relative quantity with respect to negative control treatment set to a value of 1.

(D–G) Cell proliferation (D, E), spheroid formation (F, G, upper) and colony formation (F, G, below) of HCC cells with the indicated treatments.

(H) RIP assay using anti-YTHDC1 antibody, and IgG as a negative control. The enrichment of Circ-CDYL was determined by RT−qPCR assay and agarose gel electrophoresis.

(Figures 3H, 3I, and S6B). In addition, subcutaneous injection of Circ-CDYL-overexpressing HCC cells into mice led to an increase in tumor formation and growth rate, whereas administration of STM2457 *in vivo* was able to inhibit this effect (Figures 3J and 3K).

By constructing either wild-type Circ-CDYL or mutated m^{6}A-modified sites of Circ-CDYL stably overexpressing HCC cells, we were able to confirm the HCC-promoting function of m^{6}A modification of Circ-CDYL. Notably, we found that overexpression of wild-type Circ-CDYL, but not the m^{6}A modification sites mutant equivalents, could promote spheroid growth, colony formation and cell proliferation (Figures 3L, 3M, and S6C). These data showed that METTL3-mediated m^{6}A modification of Circ-CDYL promoted HCC tumorigenesis.

m^{6}A modification of Circ-CDYL regulates its biogenesis by promoting back-splicing

Several mechanisms, including back-splicing events[24] and stabilization,[26] are used by m^{6}A modification to regulate transcript levels. We further studied the mechanism of m^{6}A-dependent upregulation of Circ-CDYL. Actinomycin D pulse-chase experiments demonstrated that neither METTL3 overexpression nor inhibition had a notable effect on the half-life of Circ-CDYL (Figure S7A). We next examined whether the m^{6}A modification regulated the back-splicing events of Circ-CDYL and found that METTL3 overexpression significantly increased Circ-CDYL expression, paralleled by a decrease in its precursor transcript (pre-CDYL) (Figure 4A, left set), while METTL3 inhibition led to the

downregulation of Circ-CDYL expression and accumulation of pre-CDYL (Figure 4A, right set). These results suggested a role of METTL3 and m^{6}A modification in the regulation of back-splicing events, which leads to the biogenesis of Circ-CDYL.

YTH domain containing 1 (YTHDC1) has been confirmed to regulate the back-splicing of circRNAs as an m^{6}A reader.[24,37] Thus, we then examined the involvement of YTHDC1 in the back-splicing of Circ-CDYL. YTHDC1 silencing (Figure S7B) in the HCCLM3 cell line resulted in a decrease in Circ-CDYL and was accompanied by an increase in pre-CDYL (Figure 4B, left set). Intriguingly, overexpression of YTHDC1 in the SMMC-7721 cell line (Figure S7C) decreased the pre-CDYL level but had a moderate effect on the level of Circ-CDYL (Figure 4B, right set). This phenomenon may be due to the low level of m^{6}A modification in SMMC-7721 cells, resulting in the limited effect of YTHDC1 alone on Circ-CDYL expression. To confirm this hypothesis, we simultaneously increased the levels of METTL3 and YTHDC1 in SMMC-7721 cells and found a significant additive effect (Figure 4C).

Functionally, as expected, we found that simultaneous overexpression of METTL3 and YTHDC1 led to enhanced stem-like properties of HCC cells as elevated expression of Circ-CDYL did, while silencing of YTHDC1 led to the opposite effects (Figures 4D–4G). Moreover, RIP-qPCR with an anti-YTHDC1 antibody revealed that Circ-CDYL was enriched in the immunoprecipitated fraction (Figure 4H), indicating that YTHDC1 binds to regions of circRNA that undergo circularization, which consistent with the results of a previous study.[24]

Briefly, these results indicated a role for METTL3 and YTHDC1-dependent m^{6}A modification in the regulation of the back-splicing reaction of Circ-CDYL, which increased the cellular expression level of Circ-CDYL by promoting its biogenesis and subsequently augmented the stem-like characteristics of HCC.

m^{6}A modification of Circ-CDYL increased the exosome sorting of Circ-CDYL, thus enhancing the stemness of recipient cells in HCC

We next examined whether m^{6}A modification affected exosomal Circ-CDYL. Consistent with the intracellular Circ-CDYL level, we also detected increased Circ-CDYL levels in exosomes derived from the METTL3-overexpressing cell line (Figure 5A, left) and decreased Circ-CDYL levels in METTL3-inhibited cells and corresponding exosomes (Figure 5B, left). Surprisingly, elevated levels of METTL3 resulted in a higher fold change in Circ-CDYL levels in exosomes than in cells (Figure 5A, right), while exosomal Circ-CDYL decreased more than cellular Circ-CDYL when METTL3 was specifically inhibited (Figure 5B, right), indicating that METTL3-dependent m^{6}A modification promoted the active sorting of Circ-CDYL into exosomes. However, ectopic overexpression of m^{6}A sites-mutated Circ-CDYL could not increase exosomal Circ-CDYL as much as the wild-type equivalent (Figure 5C), suggesting that the exosome sorting of Circ-CDYL, at least partly, is m^{6}A modification dependent.

Furthermore, LTi-Exos generated from cells with ectopic overexpression of m^{6}A sites-mutated Circ-CDYL (Circ-CDYL^{Mut} LTi-Exos) failed to elevate the Circ-CDYL level in recipient cells as LTi-Exos did (Figure 5D) and thus were unable to promote malignant proliferation, self-renewal, and colony formation of recipient HCC cells (Figures 5E and 5F). Meanwhile, LTi-Exos promoted tumorigenesis of xenografts derived from HCC cell lines *in vivo* more effectively than NLTi-Exos and Circ-CDYL^{Mut} LTi-Exos (Figure 5G). These results indicated that LTi-Exos promote the stemness of recipient cells through m^{6}A modification-dependent sorting of exosomal Circ-CDYL in HCC.

Activity of m^{6}A-modified Circ-CDYL loading into exosomes is controlled by hnRNPA2/B1

Next, we investigated the molecular machinery that regulates the sorting of Circ-CDYL into exosomes. Heterogeneous nuclear ribonucleoprotein A2/B1 (hnRNPA2/B1) has been reported as an "m^{6}A reader"[38,39] and a ubiquitous protein that controls RNA trafficking to exosomes.[40] Subsequently, we determined whether hnRNPA2/B1 controlled the loading of m^{6}A-modified Circ-CDYL into exosomes. RNA antisense purification (RAP) assays showed that hnRNPA2/B1 in HCC cells was pulled down by a probe that specifically targeted Circ-CDYL. However, m^{6}A sites-mutated Circ-CDYL could not enrich hnRNPA2/B1 effectively (Figure 6A). Moreover, specific binding of hnRNPA2/B1 to Circ-CDYL was validated by immunoprecipitation of hnRNPA2/B1 followed by RT–qPCR of Circ-CDYL (Figure 6B). Circ-CDYL was amplified from hnRNPA2/B1 but not IgG immunoprecipitates (Figure 6B), indicating an interaction between Circ-CDYL and hnRNPA2/B1 protein.

HnRNPA2/B1 silencing (Figure S7D) significantly decreased the levels of Circ-CDYL in exosomes derived from HCC cell lines with relatively high expression of Circ-CDYL (HCCLM3-and Circ-CDYL-overexpressing SMMC-7721 cells, respectively) (Figures 6C and 6D, left). Notably, the change in exosomal Circ-CDYL after hnRNPA2/B1 silencing was significant compared with that in the cellular Circ-CDYL level (Figures 6C and 6D, right), indicating that hnRNPA2/B1 could specifically stimulate the active exosome sorting of Circ-CDYL. However, when m^{6}A modification sites on Circ-CDYL were mutated (Circ-CDYL^{Mut}), hnRNPA2/B1 had a less significant effect on the exosomal level of Circ-CDYL than the wild-type equivalent (Figure 6E). These results indicated that hnRNPA2/B1 regulates the active loading of m^{6}A-modified Circ-CDYL into exosomes.

LTi-Exos hold promise for early HCC detection and surveillance

Given that Circ-CDYL plays important roles in the carcinogenesis of HCC and is specifically highly expressed in exosomes purified from the plasma of early HCC patients, we further elucidated whether Circ-CDYL could act as an early detection and surveillance biomarker for HCC in the clinic. When the diagnostic accuracy of exosomal Circ-CDYL was estimated with receiver operating characteristic (ROC) analysis in early HCC samples (Table S1), it presented an area under the curve (AUC) of 0.88 (95% CI: 0.81–0.93), with a sensitivity of 78.95% and specificity of 86.96% (Figure 7A and Table S2). Circ-CDYL expression was closely associated with EpCAM levels, as shown before (Figures 1D–1G). We next analyzed the relationship between Circ-CDYL and EpCAM in HCC clinical samples. As expected, early HCC patients had higher proportions of EpCAM$^+$ exosomes in plasma than healthy controls, which could effectively distinguish between healthy and early HCC with a sensitivity of

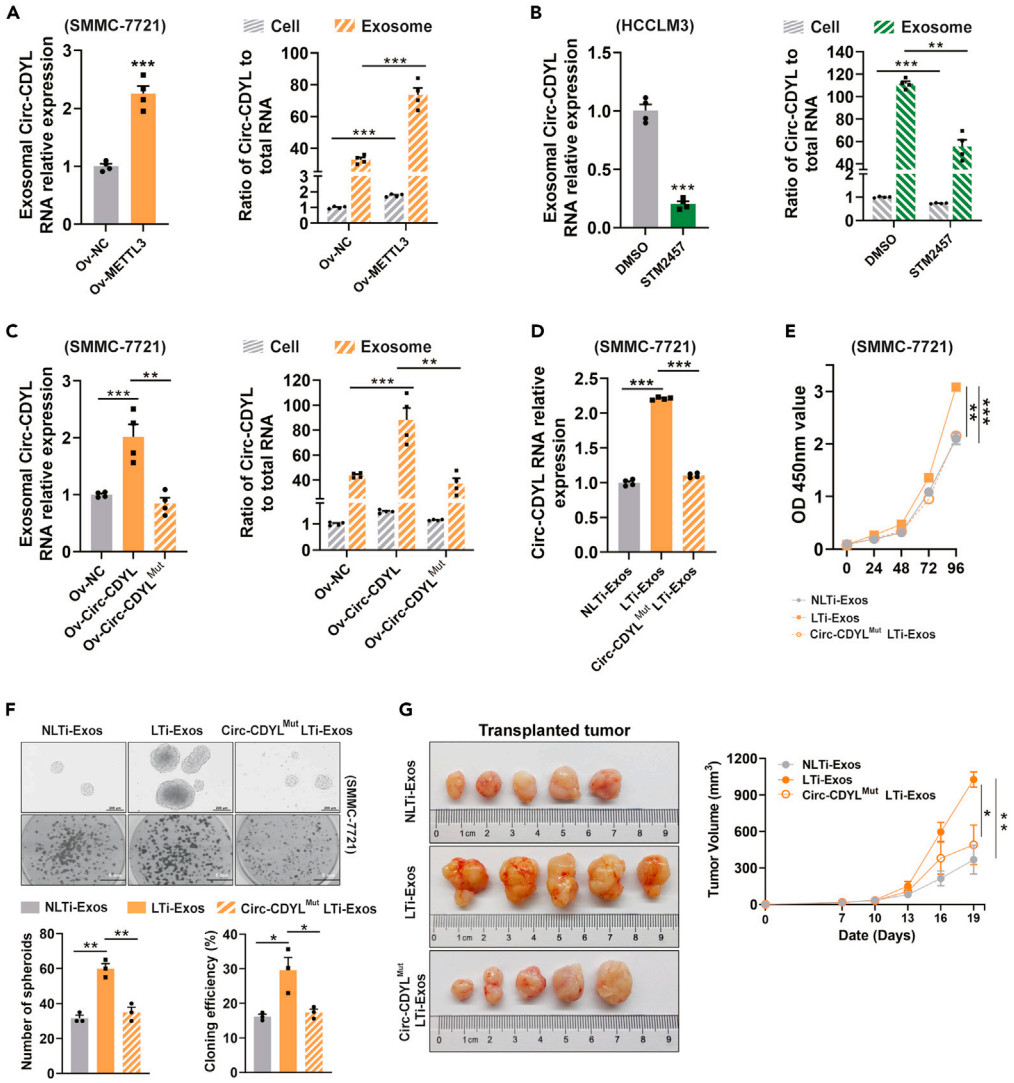

Figure 5. LTi-Exos promote the stemness of recipient cells through m^{6}A modification-dependent sorting of Circ-CDYL

(A–C) Exosomal Circ-CDYL levels were determined in METTL3-overexpressing HCC cells (Ov-METTL3) (A, left), STM2457-treated HCC cells (B, left), and HCC cells overexpressing wild-type Circ-CDYL and Circ-CDYL with m^{6}A-modified sites mutations. The ratio of cellular and exosomal Circ-CDYL to total cellular and exosomal RNA of the indicated cells, respectively, was calculated using $2^{-\Delta\Delta CT}$ from RT–qPCR (A–C, right). Ratios were normalized against β-actin and expressed as relative quantity with respect to negative control treatment set to a value of 1.

(D) The expression levels of Circ-CDYL were determined in SMMC-7721 cells after incubation with LTi-Exos derived from cells overexpressing wild-type Circ-CDYL or LTi-Exos derived from cells overexpressing m^{6}A sites-mutated Circ-CDYL (Circ-CDYL^{Mut} LTi-Exos) for 48 h.

(E and F) Determination of cell proliferation by CCK-8 assay (E), spheroid formation in low-adhesion plates (F, upper), and colony formation (F, below).

(G) SMMC-7721 cells (5×10^5) were subcutaneously injected into male nude mice. 5 μg of the indicated exosomes derived from HCC cell supernatant were intratumorally injected every 3 days after tumor cell xenograft. Representative images of tumors harvested from mice in different treatment groups 19 days after injection (left) and the tumor growth curve (right) are shown.

73.68% and specificity of 80.43% (Figures 7B and 7C). The proportions of EpCAM$^+$ exosomes were positively correlated with the exosomal level of Circ-CDYL (Figure 7D), indicating their potential synergistic effects and that these two biomarkers can be used together in clinical practice.

By integrated assessment of EpCAM$^+$ exosomes with highly expressed exosomal Circ-CDYL, this LTi-Exos biomarker enhanced the AUC to 0.88 (95% CI: 0.81–0.93), with a sensitivity of 84.21% and a specificity of 84.78% when diagnosing early HCC (Figure 7E). Comprehensive comparison of diagnostic accuracy via Youden's index (sensitivity+specificity-1) showed that the LTi-Exos biomarker, which combined the EpCAM$^+$ exosome proportion with exosomal Circ-CDYL levels, showed higher diagnostic efficacy (LTi-Exos Youden's index = 0.6899) than single factor uses (Exos Circ-CDYL Youden's index = 0.6591; EpCAM$^+$ Exos % Youden's index = 0.5411) (Table S2).

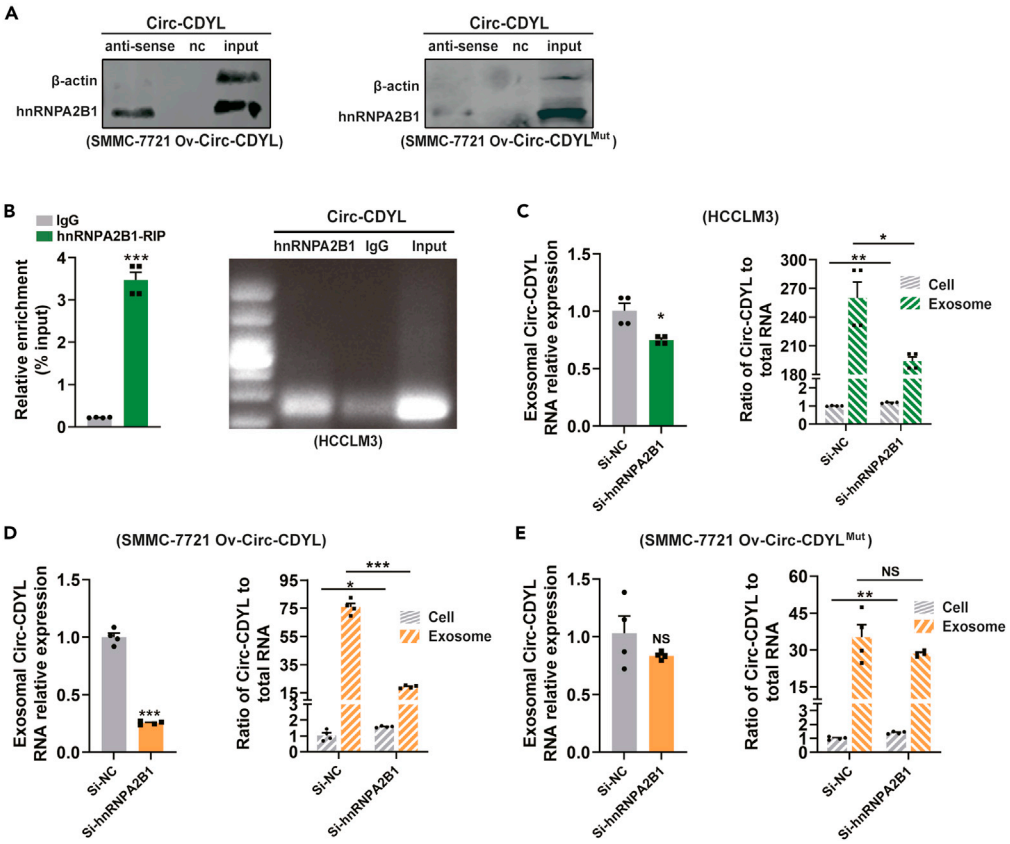

Figure 6. hnRNPA2/B1 controls the dynamic sorting of m^{6}A-modified Circ-CDYL into exosomes

(A) RNA antisense purification (RAP) assays using a biotinylated antisense probe of Circ-CDYL or negative control probe were performed using Circ-CDYL-overexpressing HCC cells (SMMC-7721 Ov-Circ-CDYL) (left), and m^{6}A sites-mutated Circ-CDYL-overexpressing HCC cells (SMMC-7721 Ov-Circ-CDYL^{Mut}) (right), followed by Western blot assays using an anti-hnRNPA2/B1 antibody.

(B) RIP assays using an anti-hnRNPA2/B1 antibody were performed. The immunoprecipitated Circ-CDYL was determined by RT–qPCR, followed by agarose gel electrophoresis.

(C–E) Exosomal Circ-CDYL levels were determined in the HCCLM3 cell line (C, left), Circ-CDYL-overexpressing HCC cells (SMMC-7721 Ov-Circ-CDYL) (D, left), and m^{6}A sites-mutated Circ-CDYL-overexpressing HCC cells (SMMC-7721 Ov-Circ-CDYL^{Mut}) (E, left) after hnRNPA2/B1 interference (Si-hnRNPA2/B1). The ratio of cellular and exosomal Circ-CDYL to total cellular and exosomal RNA of the indicated cells, respectively, was calculated using $2^{-\Delta\Delta CT}$ from RT–qPCR (C–E, right). Ratios were normalized against β-actin and expressed as relative quantity with respect to negative control treatment set to a value of 1.

α-fetoprotein (AFP), a traditional diagnostic biomarker of HCC, was also elevated in the plasma of early HCC patients in our study (Figure 7F). However, the AUC of the AFP biomarker was disappointingly low at 0.70 (95% CI: 0.62–0.77), with a sensitivity of 46.32% and specificity of 97.83% for the diagnosis of early HCC (Figure 7G). The Youden's index of AFP was lower than that of the LTi-Exos (AFP Youden's index = 0.4415; LTi-Exos Youden's index = 0.6899) (Table S2). We then combined the newly identified LTi-Exos with traditional AFP to diagnose early HCC and found that the AUC increased to the optimal 0.90 (95% CI: 0.83–0.94), with a sensitivity of 83.16% and specificity of 91.30% (Figure 7H). Logistic regression analysis also indicated that LTi-Exos combined with AFP are both independent markers for the discrimination of early HCC patients, with odds ratios (ORs) of 382.00 (95% CI: 58.38–2499.40) and 494.27 (95% CI: 74.48–3280.05), respectively (Table S2).

Taken together, LTi-Exos combined with conventional screening tools using AFP may have great promise for the early diagnosis of HCC or for surveillance of the possibility of HCC occurrence in the healthy population.

DISCUSSION

Despite the rapid development in cancer therapy, advanced HCC patients have limited therapeutic options in the clinic and thus have a poor prognosis. Fundamentally, insufficient sensitivity and specificity of the traditional surveillance test for HCC undermined the performance of early HCC diagnosis. It is noteworthy to elucidate the underlying mechanism of tumorigenesis and investigate early diagnostic and surveillance biomarkers for HCC.

By using a tissue microarray, the genome-wide differential expression of circRNAs in BCLC stage 0 HCC tissues and nontumorous adjacent tissues was analyzed. Among the identified circRNAs, Circ-CDYL was the most markedly upregulated circRNA in tumor tissues of very early

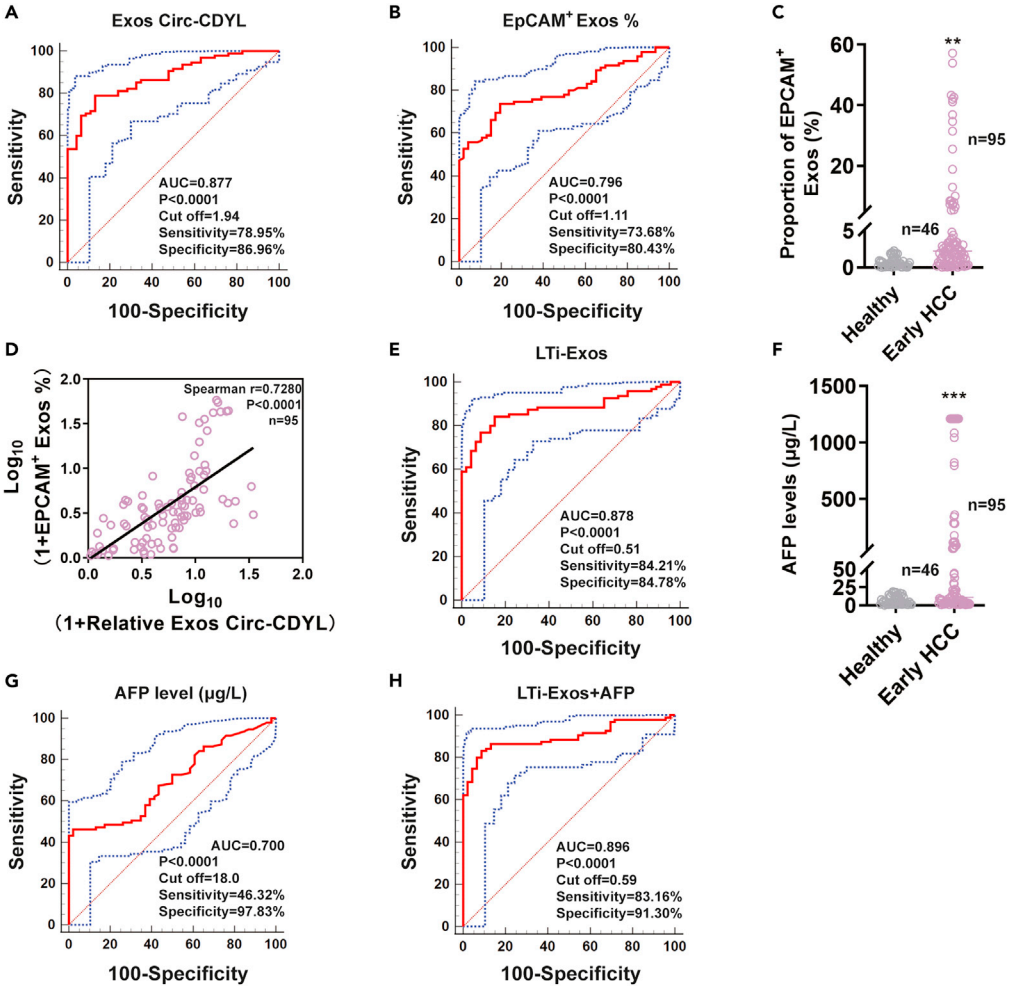

Figure 7. The combination of LTi-Exos and current screening methods based on AFP shows promise for the early detection of HCC

(A) ROC curve analysis was performed for early HCC (n = 95, 24 BCLC stage 0 HCC plus 71 BCLC stage A HCC) and healthy donors (n = 46) by estimating plasma exosomal Circ-CDYL expression.

(B) ROC curve analysis was performed for early HCC (n = 95) and healthy people (n = 46) by estimating the proportion of $EpCAM^+$ exosomes.

(C) The proportion of $EpCAM^+$ exosomes was estimated in the plasma of early HCC patients and healthy controls using flow cytometry assays.

(D) Pearson correlation analysis between exosomal Circ-CDYL expression and the proportion of $EpCAM^+$ exosomes in the plasma of early HCC (n = 95).

(E) ROC curve analysis was performed for early HCC (n = 95) and healthy donors (n = 46) by combined $EpCAM^+$ exosomes with exosomal Circ-CDYL estimating (LTi-Exos).

(F) AFP levels were estimated in the plasma of early HCC patients and healthy controls.

(G and H) ROC curve analysis was performed for early HCC patients (n = 95) and healthy donors (n = 46) by estimating the AFP level (G) and AFP combined with LTi-Exos (H).

stage HCC. The CDYL gene is located on the Y chromosome and encodes a protein that assists in gene transcription suppression and negatively regulates mammalian spermatogenesis and nervous system morphogenesis.[41,42] Circ-CDYL is generated by the head-to-tail splicing junction of the second exon of the CDYL gene. The specific high expression level of Circ-CDYL in very early stage HCC indicated a potential oncogenic function of Circ-CDYL in liver neoplasm initiation.

Exosomes are a group of extracellular vesicles that carry and transfer bioactive molecules, including circRNAs, to mediate intercellular communication. A recent study showed that tumor-derived exosomes are enriched in the plasma of patients.[43] CircRNAs were discovered to be transported by exosomes, which have been proposed as possible biomarkers for cancer.[34,43] Therefore, we investigated the extracellular release pattern of Circ-CDYL by directly studying plasma-derived exosomes from patients with early HCC. Elevated levels of Circ-CDYL were detected in exosomes isolated from early HCC patients compared with those isolated from healthy donors. These findings point to the high expression of exosomal Circ-CDYL in early HCC as a potential tool for developing a combined screening or early diagnostic biomarker for high-risk populations.

EpCAM is a popular marker of liver tumor-initiating cells.[32] An *in vitro* assay confirmed that the exosomal Circ-CDYL RNA level and EpCAM protein level were similar to those in their parental cells. Higher intracellular Circ-CDYL expression levels were detected in $EpCAM^+$ cells and undifferentiated spheroids, indicating that it may originate from liver T-ICs. Intriguingly, the proportion of $EpCAM^+$ exosomes was markedly higher than that of $EpCAM^+$ HCC cells. Furthermore, the proportion of $EpCAM^+$ exosomes increased when estimating the exosomes isolated from Circ-CDYL-overexpressing HCC cells, indicating the selective enrichment of Circ-CDYL and EpCAM cargoes sorted in producer cells before exosome release. In this study, we found that overexpression of Circ-CDYL increased the intracellular and exosomal EpCAM expression of HCC cell lines (Figure 1E). Preliminary study has been reported that EpCAM is a target of AKT/GSK-3β/β-catenin signaling pathway,[44] which driven by Circ-CDYL as shown in this study (Figure 2H). Thus, we proposed that Circ-CDYL increased the $EpCAM^+$ exosomes because exosomes derived from Circ-CDYL-overexpressed cells encapsulated more EpCAM.

Tumor-derived exosome cargoes can be transmitted into other cells, and recipient cells may subsequently take on oncogenic properties.[45] Based on the evidence that Circ-CDYL-rich and $EpCAM^+$ exosomes perform functions similar to those of liver tumor-initiating cells to promote the stem-like phenotypes of HCC, they have been termed liver tumor-initiating exosomes (LTi-Exos). We provided evidence for this concept by elevating the expression level of Circ-CDYL, increasing the proportion of $EpCAM^+$ cells, and promoting self-renewal in recipient cells after incubation with LTi-Exos. Moreover, LTi-Exos significantly promoted the malignant growth of HCC cells both *in vitro* and *in vivo*. We demonstrated in our previous study that Circ-CDYL promoted HCC by elevating the expression of HDGF and HIF1AN, which led to upregulation of C-MYC and SURVIVIN via activation of the PI3K-AKT signaling pathway and derepression of SURVIVIN transcription via the NOTCH pathway.[30] Mechanistically, LTi-Exos also activated the signal pathway that elevated intracellular expression of Circ-CDYL did.

m^6A modification is deposited by the core heterodimeric complex composed of methyltransferase-like-3 (METTL3) and −14 (METTL14), with METTL3 being the sole catalytic subunit, and it can be reversed by the m^6A demethylases FTO and ALKBH5.[23] Emerging studies have demonstrated that m^6A modifications are widespread in circRNAs, and the same m^6A "writer, reader and eraser" machinery is involved as in mRNAs.[23] MeRIP assays showed that Circ-CDYL was enriched in the m^6A-modified fraction. Bioinformatics analysis using SRAMP showed several "very high confidence" predicted m^6A sites on Circ-CDYL, among which the sites with combined score >0.7 were chosen, and were further confirmed by ligase-dependent absolute quantification analysis.

METTL3 was identified as a m^6A methyltransferase approximately three decades ago, and it is widely expressed in human tissues and plays a role in various physiological and pathological processes.[23] The elevated expression and oncogenic and cancer-promoting functions of METTL3 were reported in several types of cancer, including HCC.[23,36] For instance, METTL3 was demonstrated to promote HCC progression by inhibiting SOCS2 expression via YTHDF2[46] and was also found to regulate the epithelial-mesenchymal transition (EMT) of HCC cells by promoting the translation of SNAIL via YTHDF1.[36] In this study, we demonstrated that overexpression of METTL3 could increase the ratio of m^6A-modified Circ-CDYL and elevate the expression of Circ-CDYL, while specifically inhibiting METTL3 enzyme activity using STM2457 led to the opposite effect. As expected, METTL3 enhanced the stem-like properties of the HCC cell line, and inhibiting METTL3 using STM2457 could restrain tumor growth of HCC both *in vitro* and *in vivo*.

m^6A modification regulates various aspects of RNA at the posttranscriptional level by enlisting m^6A-reader proteins.[37] In this study, we determined that m^6A modifications can regulate the action of Circ-CDYL via two distinct mechanisms: the first involves intracellular biogenesis and the preference for either linear or back splicing of pre-CDYL, and the second involves extracellular export via encapsulation into exosomes.

YTHDF1-3 and YTHDC2 are cytoplasmic m^6A-reader proteins that regulate mRNA stability and translation, whereas YTHDC1 is located in the nucleus and has been demonstrated to regulate pre-mRNA splicing and export.[37] In particular, YTHDC1 was shown to correlate with the deposition of m^6A in specific exons on pre-mRNA.[24,26] Circ-CDYL is generated from exon 2 of its parental gene, CDYL.[30] The interaction between YTHDC1 and Circ-CDYL demonstrated by RNA Binding Protein Immunoprecipitation Assay (RIP) assay indicated that YTHDC1 may bind to exon 2 of CDYL. In agreement with previous evidence, we found that the alternative choice between linear and circular splicing of CDYL can be regulated by YTHDC1, which contributes to the increase in Circ-CDYL. Moreover, we found that YTHDC1 overexpression in SMMC-7721 cells was not able to significantly affect the back-splicing of Circ-CDYL alone, but when METTL3 and YTHDC1 were synergistically overexpressed, the back-splicing preference of Circ-CDYL was observed, emphasizing that the combined action of METTL3 and YTHDC1 is possibly required in the back-splicing reaction of Circ-CDYL.

Consistent with the cellular expression level of Circ-CDYL being positively related to its exosomal level, we found that the METTL3-dependent m^6A modification of Circ-CDYL synergistically elevated its cellular expression and exosomal levels. The ratio of exosomal to cellular Circ-CDYL levels was greatly higher in the METTL3-overexpressing HCC cell line than in the negative control cells, indicating METTL3-dependent active regulation of the sorting of Circ-CDYL to exosomes. However, cells ectopically overexpressing Circ-CDYL with mutated m^6A modification sites failed to produce exosomes with significantly higher levels of Circ-CDYL than their wild-type counterparts. LTi-Exos sorted from exosomes originating from cells ectopically overexpressing Circ-CDYL with mutated m^6A modification sites (Circ-$CDYL^{Mut}$ LTi-Exos) failed to enhance cell proliferation *in vitro* and *in vivo* and spheroid formation as well as LTi-Exos from the wild-type counterpart. Moreover, ectopic overexpression of wild-type Circ-CDYL enhanced the stemness of HCC cells, while m^6A sites-mutated Circ-CDYL failed to do so. The possible mechanisms may be as follows: (1) The active sorting of Circ-CDYL depends on its m^6A modification status. Exosomes from m^6A sites-mutated cells incorporated less Circ-CDYL than their wild-type counterparts, which may in sequence lead to lower levels of liver cancer-promoting Circ-CDYL in receiver cells than their wild-type counterparts. (2) m^6A modification of mature Circ-CDYL may be associated with cell stem-like phenotypes of liver cancer cells, so the Circ-$CDYL^{Mut}$ LTi-Exos-treated recipient cells could not develop significantly enhanced stemness as the cells uptake LTi-Exos did. 3) Both the LTi-Exos and Circ-$CDYL^{Mut}$ LTi-Exos released from the parental cells may regulate the stem-like

properties of adjacent recipient cells, leading to integrated stemness alterations in HCC cells. In any case, HCC stem-like properties may be transferred via exosomes in the tumor microenvironment.

Heterogeneous nuclear ribonucleoproteins (hnRNPs) control RNA splicing, export, modification, and localization at the transcriptional and posttranscriptional levels. In mammalian cells, hnRNP A2/B1 is a central part of the hnRNP complex. HnRNP A2/B1 controls how RNA is processed by binding to specific sequences. For example, it controls the sorting of miRNAs into exosomes by binding to specific motifs on RNA species.[47] Moreover, hnRNPA2/B1 has been demonstrated to bind to m^{6}A-modified sites in the transcriptome *in vitro* and *in vivo* and is regarded as an "m^{6}A reader".[38] However, whether it can regulate the exosome sorting of m^{6}A-modified circRNA is still not quite clear. Here, we found that m^{6}A sites-mutated Circ-CDYL could not be effectively encapsulated into exosomes as wild-type Circ-CDYL, which further supports the m^{6}A-dependent exosome sorting of Circ-CDYL. Furthermore, we found that less Circ-CDYL was packaged into exosomes in HCC cells after hnRNPA2/B1 interference, while hnRNPA2/B1 could not effectively regulate the exosome sorting of m^{6}A sites-mutated Circ-CDYL as it did wild-type Circ-CDYL, indicating that hnRNPA2/B1 controls the exosome sorting of Circ-CDYL in a m^{6}A modification-dependent mechanism. Recently, other research suggested that hnRNPA2/B1 regulates m^{6}A-modified RNAs without binding to the m^{6}A motif directly, which made it an "m^{6}A switch" rather than an "m^{6}A reader".[48] Uncovering the underlying mechanism of how hnRNPA2/B1 binds with and regulates m^{6}A-bearing transcripts requires further study.

Exosomes have the appealing potential to be optimal biomarkers for screening diseases, including cancer, due to their reflection of both the genotype and phenotype of parental cells.[43] Thus, we further investigated the possibility of early HCC diagnosis and surveillance utilizing these LTi-Exos. After analyzing the exosomes isolated from the plasma of BCLC stage 0 and stage A HCC patients, we proved the significantly higher proportion of EpCAM$^+$ exosomes and elevated Circ-CDYL and AFP levels in early HCC patients. The LTi-Exos reached an AUC of 0.88, with a sensitivity of 84.21% and specificity of 84.78% when diagnosing early HCC. The diagnostic accuracy of LTi-Exos is better than that of traditional AFP, with an AUC of 0.70 and a sensitivity of 46.32%. When LTi-Exos were combined with AFP, BCLC stage 0/A HCC patient samples could be distinguished from healthy subjects with 83.16% sensitivity and 91.30% specificity, and the AUC was enhanced to optimal 0.90.

Collectively, we identified the oncogenic effects of METTL3-dependent m^{6}A modification of Circ-CDYL in HCC. On the one hand, Circ-CDYL m^{6}A modification elevates its cellular expression by promoting the back-splicing of Circ-CDYL via YTHDC1; on the other hand, Circ-CDYL m^{6}A modification increases the exosomal level of Circ-CDYL by promoting the active sorting of Circ-CDYL into exosomes via hnRNPA2/B1, which increases the level of Circ-CDYL in recipient cells by regulating the tumor microenvironment. These two mechanisms synergistically contribute to cancer initiation and progression. Circ-CDYL-enriched and EpCAM-positive LTi-Exos could be a potential biomarker for early HCC detection. Combining these newly identified LTi-Exos with traditional AFP would be of great possibility for the early diagnosis of HCC by liquid biopsy. Furthermore, it may be used as a surveillance indicator for the healthy or high-risk population of liver cancer in the future.

Limitations of the study

There are also several limitations to our study, including the fact that we did not investigate how each m^{6}A-modified site on Circ-CDYL contributes to its back-splicing and exosomes sorting. Future relevant research will be conducted.

STAR★METHODS

Detailed methods are provided in the online version of this paper and include the following:

- KEY RESOURCES TABLE
- RESOURCE AVAILABILITY
  - Lead contact
  - Materials availability
  - Data and code availability
- EXPERIMENTAL MODEL AND STUDY PARTICIPANT DETAILS
  - HCC patients and clinical samples
  - Animals
  - Cell lines and cell culture
  - *In vivo* xenograft experiments
  - Ethics approval and consent to participate
- METHOD DETAILS
  - RNA antisense purification (RAP) assay
  - M^{6}A-RNA binding protein immunoprecipitation (meRIP) assay
  - Ligase-dependent absolute quantification of the m^{6}A modification fraction at specific sites in RNAs
  - MazF-dependent quantification of m^{6}A modification in RNAs
  - CCK8, spheroid formation, and colony formation assays
  - Lentiviral infection
  - siRNA transfection
  - STM2457 treatment
  - Flow cytometry analysis of cells

- Western blot
- Actinomycin D treatment
- RNA isolation and PCR analysis

- QUANTIFICATION AND STATISTICAL ANALYSIS

SUPPLEMENTAL INFORMATION

Supplemental information can be found online at https://doi.org/10.1016/j.isci.2023.108022.

ACKNOWLEDGMENTS

We gratefully acknowledge the support from the State Key Project on Infectious Diseases of China (2018ZX10723204-002-002), National Natural Science Foundation of China (82172896, 91859205, 81988101, 81830054, 81902940, 81902942), Natural Science Foundation of Shanghai (19ZR1400300), Shanghai Top Young Talents Program, Foundation of Shanghai Shenkang Hospital Development Center (SHDC2020CR2011A, SHDC12016127), Shanghai Key Laboratory of Hepato-biliary Tumor Biology, The Key Laboratory of Signaling Regulation and Targeting Therapy of Liver Cancer (SMMU), Ministry of Education, Shanghai, China. We would like to thank Yanting Yu, Qinyun Huang, Shanhua Tang, Linna Guo, Dan Cao for technical assistance.

AUTHOR CONTRIBUTIONS

H.Y.W. contributed to study concept design and supervised all works; L.L. and Y.X.T. contributed to the analysis and interpretation of data and drafting of the paper. Y.P.W. and J.B.F. contributed to the acquisition of data, H.Z. and Y.L. contributed to the acquisition of clinical samples. X.W.T., S.W.L., M.Y., F.Y.L., G.K.Z., H.H.Q., K.C.Z., P.H.Y., X.W.Y., Q.Y., S.N.G., and B.H.Z. contributed to technical and material support. All authors have read and approved the article.

DECLARATION OF INTERESTS

The authors declare that they have no competing interests.

Received: January 28, 2023
Revised: July 13, 2023
Accepted: September 19, 2023
Published: October 13, 2023

REFERENCES

1. Torre, L.A., Bray, F., Siegel, R.L., Ferlay, J., Lortet-Tieulent, J., and Jemal, A. (2015). Global cancer statistics, 2012. CA. Cancer J. Clin. *65*, 87–108.
2. Li, L., Chen, J., Chen, X., Tang, J., Guo, H., Wang, X., Qian, J., Luo, G., He, F., Lu, X., et al. (2016). Serum miRNAs as predictive and preventive biomarker for pre-clinical hepatocellular carcinoma. Cancer Lett. *373*, 234–240.
3. Forner, A., Reig, M.E., de Lope, C.R., and Bruix, J. (2010). Current strategy for staging and treatment: the BCLC update and future prospects. Semin. Liver Dis. *30*, 61–74.
4. Canelo, R., Hakim, N.S., and Ringe, B. (2003). Experience with hystidine tryptophan ketoglutarate versus University Wisconsin preservation solutions in transplantation. Int. Surg. *88*, 145–151.
5. Llovet, J.M., Fuster, J., and Bruix, J. (1999). Intention-to-treat analysis of surgical treatment for early hepatocellular carcinoma: resection versus transplantation. Hepatology *30*, 1434–1440.
6. Cillo, U., Vitale, A., Grigoletto, F., Farinati, F., Brolese, A., Zanus, G., Neri, D., Boccagni, P., Srsen, N., D'Amico, F., et al. (2006). Prospective validation of the Barcelona Clinic Liver Cancer staging system. J. Hepatol. *44*, 723–731.
7. Forner, A. (2015). Hepatocellular carcinoma surveillance with miRNAs. Lancet Oncol. *16*, 743–745.
8. Poon, D., Anderson, B.O., Chen, L.T., Tanaka, K., Lau, W.Y., Van Cutsem, E., Singh, H., Chow, W.C., Ooi, L.L., Chow, P., et al. (2009). Management of hepatocellular carcinoma in Asia: consensus statement from the Asian Oncology Summit 2009. Lancet Oncol. *10*, 1111–1118.
9. Gebo, K.A., Chander, G., Jenckes, M.W., Ghanem, K.G., Herlong, H.F., Torbenson, M.S., El-Kamary, S.S., and Bass, E.B. (2002). Screening tests for hepatocellular carcinoma in patients with chronic hepatitis C: a systematic review. Hepatology *36* (5 Suppl 1), S84–S92.
10. Zinkin, N.T., Grall, F., Bhaskar, K., Otu, H.H., Spentzos, D., Kalmowitz, B., Wells, M., Guerrero, M., Asara, J.M., Libermann, T.A., and Afdhal, N.H. (2008). Serum proteomics and biomarkers in hepatocellular carcinoma and chronic liver disease. Clin. Cancer Res. *14*, 470–477.
11. Marrero, J.A., Feng, Z., Wang, Y., Nguyen, M.H., Befeler, A.S., Roberts, L.R., Reddy, K.R., Harnois, D., Llovet, J.M., Normolle, D., et al. (2009). Alpha-fetoprotein, des-gamma carboxyprothrombin, and lectin-bound alpha-fetoprotein in early hepatocellular carcinoma. Gastroenterology *137*, 110–118.
12. Wang, Y., Liu, J., Ma, J., Sun, T., Zhou, Q., Wang, W., Wang, G., Wu, P., Wang, H., Jiang, L., et al. (2019). Exosomal circRNAs: biogenesis, effect and application in human diseases. Mol. Cancer *18*, 116.
13. Li, S., Li, Y., Chen, B., Zhao, J., Yu, S., Tang, Y., Zheng, Q., Li, Y., Wang, P., He, X., and Huang, S. (2018). exoRBase: a database of circRNA, lncRNA and mRNA in human blood exosomes. Nucleic Acids Res. *46*, D106–D112.
14. Yang, P., Song, F., Yang, X., Yan, X., Huang, X., Qiu, Z., Wen, Z., Liang, C., Xin, X., Lei, Z., et al. (2022). Exosomal MicroRNA Signature Acts as an Efficient Biomarker for Non-Invasive Diagnosis of Gallbladder Carcinoma. iScience *25*, 104816.
15. Hoshino, A., Costa-Silva, B., Shen, T.L., Rodrigues, G., Hashimoto, A., Tesic Mark, M., Molina, H., Kohsaka, S., Di Giannatale, A., Ceder, S., et al. (2015). Tumour exosome integrins determine organotropic metastasis. Nature *527*, 329–335.
16. Costa-Silva, B., Aiello, N.M., Ocean, A.J., Singh, S., Zhang, H., Thakur, B.K., Becker, A., Hoshino, A., Mark, M.T., Molina, H., et al. (2015). Pancreatic cancer exosomes initiate pre-metastatic niche formation in the liver. Nat. Cell Biol. *17*, 816–826.
17. Lin, J., Wang, X., Zhai, S., Shi, M., Peng, C., Deng, X., Fu, D., Wang, J., and Shen, B. (2022). Hypoxia-induced exosomal circPDK1 promotes pancreatic cancer glycolysis via c-myc activation by modulating miR-628-3p/BPTF axis and degrading BIN1. J. Hematol. Oncol. *15*, 128.
18. Movahedpour, A., Khatami, S.H., Karami, N., Vakili, O., Naeli, P., Jamali, Z., Shabaninejad,

Z., Tazik, K., Behrouj, H., and Ghasemi, H. (2022). Exosomal noncoding RNAs in prostate cancer. Clin. Chim. Acta *537*, 127–132.
19. Rackles, E., Lopez, P.H., and Falcon-Perez, J.M. (2022). Extracellular vesicles as source for the identification of minimally invasive molecular signatures in glioblastoma. Semin. Cancer Biol. *87*, 148–159.
20. Rybak-Wolf, A., Stottmeister, C., Glažar, P., Jens, M., Pino, N., Giusti, S., Hanan, M., Behm, M., Bartok, O., Ashwal-Fluss, R., et al. (2015). Circular RNAs in the Mammalian Brain Are Highly Abundant, Conserved, and Dynamically Expressed. Mol. Cell *58*, 870–885.
21. Salzman, J., Chen, R.E., Olsen, M.N., Wang, P.L., and Brown, P.O. (2013). Cell-type specific features of circular RNA expression. PLoS Genet. *9*, e1003777.
22. Jeck, W.R., and Sharpless, N.E. (2014). Detecting and characterizing circular RNAs. Nat. Biotechnol. *32*, 453–461.
23. Huang, H., Weng, H., and Chen, J. (2020). m^6A Modification in Coding and Non-coding RNAs: Roles and Therapeutic Implications in Cancer. Cancer Cell *37*, 270–288.
24. Di Timoteo, G., Dattilo, D., Centrón-Broco, A., Colantoni, A., Guarnacci, M., Rossi, F., Incarnato, D., Oliviero, S., Fatica, A., Morlando, M., and Bozzoni, I. (2020). Modulation of circRNA Metabolism by m^6A Modification. Cell Rep. *31*, 107641.
25. Chen, R.X., Chen, X., Xia, L.P., Zhang, J.X., Pan, Z.Z., Ma, X.D., Han, K., Chen, J.W., Judde, J.G., Deas, O., et al. (2019). N6-methyladenosine modification of circNSUN2 facilitates cytoplasmic export and stabilizes HMGA2 to promote colorectal liver metastasis. Nat. Commun. *10*, 4695.
26. Park, O.H., Ha, H., Lee, Y., Boo, S.H., Kwon, D.H., Song, H.K., and Kim, Y.K. (2019). Endoribonucleolytic Cleavage of m^6A-Containing RNAs by RNase P/MRP Complex. Mol. Cell *74*, 494–507.e8.
27. Yang, Y., Fan, X., Mao, M., Song, X., Wu, P., Zhang, Y., Jin, Y., Yang, Y., Chen, L.L., Wang, Y., et al. (2017). Extensive translation of circular RNAs driven by N6-methyladenosine. Cell Res. *27*, 626–641.
28. Zuo, X., Chen, Z., Gao, W., Zhang, Y., Wang, J., Wang, J., Cao, M., Cai, J., Wu, J., and Wang, X. (2020). M^6A-mediated upregulation of LINC00958 increases lipogenesis and acts as a nanotherapeutic target in hepatocellular carcinoma. J. Hematol. Oncol. *13*, 5.
29. Peng, H., Chen, B., Wei, W., Guo, S., Han, H., Yang, C., Ma, J., Wang, L., Peng, S., Kuang, M., and Lin, S. (2022). N6-methyladenosine (m^6A) in 18S *r*RNA promotes fatty acid metabolism and oncogenic transformation. Nat. Metab. *4*, 1041–1054.
30. Wei, Y., Chen, X., Liang, C., Ling, Y., Yang, X., Ye, X., Zhang, H., Yang, P., Cui, X., Ren, Y., et al. (2020). A Noncoding Regulatory RNAs Network Driven by Circ-CDYL Acts Specifically in the Early Stages Hepatocellular Carcinoma. Hepatology *71*, 130–147.
31. Ma, S., Chan, K.W., Hu, L., Lee, T.K.W., Wo, J.Y.H., Ng, I.O.L., Zheng, B.J., and Guan, X.Y. (2007). Identification and characterization of tumorigenic liver cancer stem/progenitor cells. Gastroenterology *132*, 2542–2556.
32. Yamashita, T., Ji, J., Budhu, A., Forgues, M., Yang, W., Wang, H.Y., Jia, H., Ye, Q., Qin, L.X., Wauthier, E., et al. (2009). EpCAM-positive hepatocellular carcinoma cells are tumor-initiating cells with stem/progenitor cell features. Gastroenterology *136*, 1012–1024.
33. Lee, T.K.W., Castilho, A., Cheung, V.C.H., Tang, K.H., Ma, S., and Ng, I.O.L. (2011). CD24(+) liver tumor-initiating cells drive self-renewal and tumor initiation through STAT3-mediated NANOG regulation. Cell Stem Cell *9*, 50–63.
34. Li, C., Ni, Y.Q., Xu, H., Xiang, Q.Y., Zhao, Y., Zhan, J.K., He, J.Y., Li, S., and Liu, Y.S. (2021). Roles and mechanisms of exosomal non-coding RNAs in human health and diseases. Signal Transduct. Target. Ther. *6*, 383.
35. Csepany, T., Lin, A., Baldick, C.J., Jr., and Beemon, K. (1990). Sequence specificity of mRNA N6-adenosine methyltransferase. J. Biol. Chem. *265*, 20117–20122.
36. Lin, X., Chai, G., Wu, Y., Li, J., Chen, F., Liu, J., Luo, G., Tauler, J., Du, J., Lin, S., et al. (2019). RNA m^6A methylation regulates the epithelial mesenchymal transition of cancer cells and translation of Snail. Nat. Commun. *10*, 2065.
37. Zaccara, S., Ries, R.J., and Jaffrey, S.R. (2019). Reading, writing and erasing mRNA methylation. Nat. Rev. Mol. Cell Biol. *20*, 608–624.
38. Alarcón, C.R., Goodarzi, H., Lee, H., Liu, X., Tavazoie, S., and Tavazoie, S.F. (2015). HNRNPA2B1 Is a Mediator of m(6)A-Dependent Nuclear RNA Processing Events. Cell *162*, 1299–1308.
39. Jiang, F., Tang, X., Tang, C., Hua, Z., Ke, M., Wang, C., Zhao, J., Gao, S., Jurczyszyn, A., Janz, S., et al. (2021). HNRNPA2B1 promotes multiple myeloma progression by increasing AKT3 expression via m^6A-dependent stabilization of ILF3 mRNA. J. Hematol. Oncol. *14*, 54.
40. Pan, Z., Zhao, R., Li, B., Qi, Y., Qiu, W., Guo, Q., Zhang, S., Zhao, S., Xu, H., Li, M., et al. (2022). EWSR1-induced circNEIL3 promotes glioma progression and exosome-mediated macrophage immunosuppressive polarization via stabilizing IGF2BP3. Mol. Cancer *21*, 16.
41. Mulligan, P., Westbrook, T.F., Ottinger, M., Pavlova, N., Chang, B., Macia, E., Shi, Y.J., Barretina, J., Liu, J., Howley, P.M., et al. (2008). CDYL bridges REST and histone methyltransferases for gene repression and suppression of cellular transformation. Mol. Cell *32*, 718–726.
42. Qi, C., Liu, S., Qin, R., Zhang, Y., Wang, G., Shang, Y., Wang, Y., and Liang, J. (2014). Coordinated regulation of dendrite arborization by epigenetic factors CDYL and EZH2. J. Neurosci. *34*, 4494–4508.
43. Li, Y., Zheng, Q., Bao, C., Li, S., Guo, W., Zhao, J., Chen, D., Gu, J., He, X., and Huang, S. (2015). Circular RNA is enriched and stable in exosomes: a promising biomarker for cancer diagnosis. Cell Res. *25*, 981–984.
44. Zhang, P.P., Wang, P.Q., Qiao, C.P., Zhang, Q., Zhang, J.P., Chen, F., Zhang, X., Xie, W.F., Yuan, Z.L., Li, Z.S., and Chen, Y.X. (2016). Differentiation therapy of hepatocellular carcinoma by inhibiting the activity of AKT/GSK-3β/β-catenin axis and TGF-β induced EMT with sophocarpine. Cancer Lett. *376*, 95–103.
45. Qu, L., Ding, J., Chen, C., Wu, Z.J., Liu, B., Gao, Y., Chen, W., Liu, F., Sun, W., Li, X.F., et al. (2016). Exosome-Transmitted lncARSR Promotes Sunitinib Resistance in Renal Cancer by Acting as a Competing Endogenous RNA. Cancer Cell *29*, 653–668.
46. Chen, M., Wei, L., Law, C.T., Tsang, F.H.C., Shen, J., Cheng, C.L.H., Tsang, L.H., Ho, D.W.H., Chiu, D.K.C., Lee, J.M.F., et al. (2018). RNA N6-methyladenosine methyltransferase-like 3 promotes liver cancer progression through YTHDF2-dependent posttranscriptional silencing of SOCS2. Hepatology *67*, 2254–2270.
47. Villarroya-Beltri, C., Gutiérrez-Vázquez, C., Sánchez-Cabo, F., Pérez-Hernández, D., Vázquez, J., Martin-Cofreces, N., Martinez-Herrera, D.J., Pascual-Montano, A., Mittelbrunn, M., and Sánchez-Madrid, F. (2013). Sumoylated hnRNPA2B1 controls the sorting of miRNAs into exosomes through binding to specific motifs. Nat. Commun. *4*, 2980.
48. Wu, B., Su, S., Patil, D.P., Liu, H., Gan, J., Jaffrey, S.R., and Ma, J. (2018). Molecular basis for the specific and multivariant recognitions of RNA substrates by human hnRNP A2/B1. Nat. Commun. *9*, 420.
49. Schneider, C.A., Rasband, W.S., and Eliceiri, K.W. (2012). NIH Image to ImageJ: 25 years of image analysis. Nat Methods *9*, 671–675.
50. Théry, C., Amigorena, S., Raposo, G., and Clayton, A. (2006). Isolation and characterization of exosomes from cell culture supernatants and biological fluids. Curr. Protoc. Cell Biol.. Chapter 3: Unit 3.22.
51. Theodoraki, M.N., Yerneni, S.S., Hoffmann, T.K., Gooding, W.E., and Whiteside, T.L. (2018). Clinical significance of PD-L1$^+$ exosomes in plasma of head and neck cancer patients. Clin. Cancer Res. *24*, 896–905.

STAR★METHODS

KEY RESOURCES TABLE

REAGENT or RESOURCE	SOURCE	IDENTIFIER
Antibodies		
anti-m^{6}A antibody	Synaptic Systems	Cat#202003; RRID:AB_2279214
biotin-labeled anti-CD63 mAb	Biolegend	Cat#353018; RRID:AB_2561676
fluorescein-conjugated anti-EpCAM APC	Biolegend	Cat#369810; RRID:AB_2650907
fluorescein-conjugated anti-CD133-APC	Biolegend	Cat#397906; RRID:AB_2876721
fluorescein-conjugated anti-CD24-APC	Biolegend	Cat#382604; RRID:AB_2927986
isotype control antibody	Biolegend	Cat#400222; RRID:AB_2891178
rabbit polyclonal anti-CD63	Proteintech	Cat#25682-1-AP; RRID:AB_2783831
rabbit monoclonal anti-EpCAM	AbCAM	Cat#ab32392; RRID:AB_732181
rabbit monoclonal anti-HDGF	AbCAM	Cat#ab131046; RRID:AB_11156674
mouse mAb anti-PI3K (P85α)	Cell Signaling Technology	Cat#13666S; RRID:AB_2798288
rabbit mAb anti-PI3K (P110β)	Cell Signaling Technology	Cat#3011S; RRID:AB_2165246
rabbit monoclonal anti-p-Akt (Ser473)	Cell Signaling Technology	Cat#4060S; RRID:AB_2315049
rabbit monoclonal anti-p-Akt (Thr308)	Cell Signaling Technology	Cat#13038S; RRID:AB_2629447
rabbit monoclonal anti-AKT (pan)	Cell Signaling Technology	Cat#4691P; RRID:AB_915783
rabbit monoclonal anti-C-MYC	Cell Signaling Technology	Cat#13987S; RRID:AB_2631168
rabbit monoclonal anti-p-mTOR (Ser2448)	Cell Signaling Technology	Cat#5536P; RRID:AB_10691552
rabbit monoclonal anti-mTOR	Cell Signaling Technology	Cat#2983P; RRID:AB_2105622
rabbit polyclonal anti-p-GSK-3β (Ser9)	Abclonal	Cat#AP0358; RRID:AB_2771152
rabbit polyclonal anti-GSK-3β	Abclonal	Cat#A0479; RRID:AB_2757212
mouse polyclonal anti-HIF1AN	Santa Cruz	Cat#SC-271780; RRID:AB_10709435
rabbit polyclonal anti-SURVIVIN	Proteintech	Cat#10508-1-AP; RRID:AB_2064048
rabbit monoclonal anti-METTL3	Cell Signaling Technology	Cat#86132; RRID:AB_2800072
rabbit monoclonal anti-YTHDC1	Cell Signaling Technology	Cat#77422; RRID:AB_2799899
mouse monoclonal anti-hnRNPA2B1	Cell Signaling Technology	Cat#9304; RRID:AB_10694208
rabbit monoclonal anti-β-actin	Abclonal	Cat#AC026; RRID:AB_2768234
mouse monoclonal anti-GAPDH	Santa Cruz	Cat#SC-47724; RRID:AB_627678
mouse fluorescein-conjugated secondary antibody	Li-Cor	Cat#C926-32210; RRID:AB_621842
rabbit fluorescein-conjugated secondary antibody	Li-Cor	Cat#926-32211; RRID:AB_621843
Bacterial and virus strains		
Circ-CDYL overexpression lentivirus	GeneChem	N/A
METTL3 overexpression lentivirus	Heyuan Biotechnology	N/A
YTHDC1 overexpression lentivirus	Heyuan Biotechnology	N/A
Biological samples		
Human plasma using for exosomes analysis	Eastern Hepatobiliary Surgery Hospital	N/A
Chemicals, peptides, and recombinant proteins		
TRIzol Reagent	Invitrogen	Cat#15596026
STM2457	MedChemExpress	Cat#HY-134836
Actinomycin D	MedChemExpress	Cat#HY-17559
DAPI	Beyotime	Cat# C1002
Protease inhibitor cocktail and phosphatase inhibitor	Beyotime	Cat# P1046

(*Continued on next page*)

Continued

REAGENT or RESOURCE	SOURCE	IDENTIFIER
Western and IP buffer	Beyotime	Cat# P0013
DMEM	BasalMedia	Cat#L110KJ
Fetal Bovine Serum	Biological Industries	Cat#04-001-1ACS
Critical commercial assays		
RNA Antisense Purification Kit	BersinBio	Cat#Bes5103
Magna RIP RNA-binding protein immunoprecipitation kit	Millipore	Cat#17-700
Dynabeads kilobase BINDER kit	Invitrogen	Cat#60101
Cell counting kit-8 (CCK-8)	Dojindo	Cat#Cat# CK04
JetPRIME reagents	Poly plus	Cat#114-15
exoEasy Maxi Kit	Qiagen	Cat#76064
iScript™ cDNA Synthesis Kit	Bio-Rad	Cat#1708891
PKH26 kit	Wayenbio	Cat#ESQ-R-001
Actin-Tracker Green	Beyotime	Cat#C1033
Experimental models: Cell lines		
HCCLM3	Cell Bank of Type Culture Collection of the Chinese Academy of Sciences	N/A
SMMC-7721	Cell Bank of Type Culture Collection of the Chinese Academy of Sciences	N/A
Experimental models: Organisms/strains		
Mouse: BALB/c-Nude	GemPharmatech Co.	D000521
Oligonucleotides		
Circ-CDYL RAP Probe sequence: Circ-CDYL1: TTCAACCTTTCCCGTTAACA-3′bio Circ-CDYL2: ACAATCCTTTCAACCTTTCC-3′bio	RiboBio	N/A
NC siRNA: sense: UUCUCCGAACGUGUCACGUdTdT antisense: ACGUGACACGUUCGGAGAAdTdT	Biotend Co.	N/A
YTHDC1 siRNA 1#: sense: ACGUCUAUCCACUUCAAGCCCdTdT antisense: GCUUGAAGUGGAUAGACGUGCdTdT	Biotend Co.	N/A
YTHDC1 siRNA 2#: sense: AUACAGAUUGGAUUACGGCUGdTdT antisense: GCCGUAAUCCAAUCUGUAUUUdTdT	Biotend Co.	N/A
HnRNPA2B1 siRNA 1#: sense: GGCUUUGUCUAGACAAGAAdTdT antisense: UUCUUGUCUAGACAAAGCCdTdT	Biotend Co.	N/A
HnRNPA2B1 siRNA 2#: sense: GCUGCAAGACCUCAUUCAAdTdT antisense: UUGAAUGAGGUCUUGCAGCdTdT	Biotend Co.	N/A
HnRNPA2B1 siRNA 2#: sense: GGACCAGGAAGUAACUUUAdTdT antisense: UAAAGUUACUUCCUGGUCCdTdT	Biotend Co.	N/A
Recombinant DNA		
Circ-CDYL overexpression, see STAR Methods	GeneChem	N/A
Circ-CDYL^{mut} overexpression, see STAR Methods	GeneChem	N/A
EpCAM-mCherry fusion overexpression, see STAR Methods	GeneChem	N/A

(*Continued on next page*)

Continued

REAGENT or RESOURCE	SOURCE	IDENTIFIER
METTL3 overexpression, see STAR Methods	Heyuan Biotechnology	N/A
YTHDC1 overexpression, see STAR Methods	Heyuan Biotechnology	N/A
Software and algorithms		
ImageJ	Schneider et al.[49]	https://imagej.nih.gov/ij/
GraphPad Prism 9	Graphpad Software	https://www.graphpad.com
FlowJo	BD Biosciences Pharmingen	https://www.bdbiosciences.com
BioTek Gen5 system	BioTeck	N/A
LightCycler® 96 Real-Time PCR System	Roche	N/A
Other		
Mastercycler	Eppendorf	Nexus GSX1

RESOURCE AVAILABILITY

Lead contact

Further information and requests for resources and reagents should be directed to and will be fulfilled by the lead contact, Prof. Hongyang Wang (hywangk@vip.sina.com).

Materials availability

This study did not generate new unique reagents.

Data and code availability

All data reported in this paper will be shared by the lead contact upon request.
This paper does not report original code.
Any additional information required to reanalyze the data reported in this paper is available from the lead contact upon request.

EXPERIMENTAL MODEL AND STUDY PARTICIPANT DETAILS

HCC patients and clinical samples

Early HCC patients' plasma using for exosomes analysis in this study were obtained from patients who were diagnosed and received surgical resection at the Eastern Hepatobiliary Surgery Hospital, Shanghai, China. No patients received any preoperative anticancer treatment. All of these patients are Chinese (Asian), including 77 males and 18 females. The ages of these patients ranged from 30 to 70, with a mean age of 60. Detailed patient information is shown in Table S1.

HCC staging was determined by the Barcelona Clinic Liver Cancer staging system (BCLC). BCLC stage 0 HCC (very early stage HCC) was defined as a single lesion <2 cm without vascular involvement or metastasis. BCLC stage A HCC (early stage HCC) is defined by a single lesion between 2 and 5 cm or $\leq$3 lesions each <3 cm, without portal vein thrombosis or extrahepatic metastasis. Late-stage HCC was defined as the combination of intermediate (BCLC stage B HCC) or advanced HCC (BCLC stage C HCC). All research complied with the principles of the Declaration of Helsinki. Patient samples were obtained following informed consent according to an established protocol approved by the Ethics Committee of Eastern Hepatobiliary Surgery Hospital.

Animals

The 4–6 weeks old male nude mice were housed in individual microisolator cages with free access to sterile water and irradiated normal food in a specific pathogen-free facility. Experiments were conducted by following the criteria outlined in the Guide for the Care and Use of Laboratory Animals, prepared by the National Academy of Sciences and published by the National Institutes of Health (NIH publication 86-23; revised 1985). All animal care protocols and experiments were reviewed and approved by the Animal Care and Use Committee of the Laboratory Animal Research Center at the Eastern Hepato-biliary Surgery Hospital, Second Military Medical University.

Cell lines and cell culture

The HCC cell lines HCCLM3 and SMMC-7721 were obtained from Cell Bank of Type Culture Collection of the Chinese Academy of Sciences (Shanghai Institute of Cell Biology), and cultured at 37°C in an atmosphere containing 5% CO_2 and routinely cultured in DMEM supplemented with 10% fetal bovine serum. Cells were passaged every 1-2 d to maintain logarithmic growth.

In vivo xenograft experiments

For the exosome *in vitro* treatment experiment, a total of 5×10^5 SMMC-7721 cells were injected subcutaneously into the flanks of male nude mice (4–6 weeks old, n = 6) after 48 hours of incubation with 1 μg of LTi-Exos or NLTi-Exos. The subcutaneous tumors were harvested 3 weeks after injection.

For the exosome *in vivo* treatment experiment, a total of 5×10^5 SMMC-7721 cells were injected subcutaneously into the flanks of male nude mice (4–6 weeks old, n = 5). Then, 5 μg of LTi-Exos or NLTi-Exos were injected intratumorally every 3 days after xenograft implantation. The subcutaneous tumors were harvested 19 days after injection. Tumor volume was calculated as follows: V (mm^3) = $width^2$ (mm^2) × length (mm)/2.

Ethics approval and consent to participate

All research complied with the principles of the Declaration of Helsinki. Patient samples were obtained following informed consent according to an established protocol approved by the Ethics Committee of Eastern Hepatobiliary Surgery Hospital. All animal care protocols and experiments were reviewed and approved by the Animal Care and Use Committee of the Laboratory Animal Research Center at the Eastern Hepato-biliary Surgery Hospital, Second Military Medical University.

METHOD DETAILS

RNA antisense purification (RAP) assay

For the RAP assay, an RNA Antisense Purification Kit (Bes5103, BersinBio, Guangzhou, China) was utilized. Biotinylated probes for Circ-CDYL and a negative control probe were produced by RiboBio Co. (Guangzhou, China).

RAP assays were performed according to the previous study.[30] For each RAP experiment, lysate from $2*10^8$ cells, 40 pmol of probe, and 40 μL streptavidin-coated beads were used. HCC cell lines were crosslinked with 1 mg/mL 4′-aminomethyltrioxalen (AMT), a psoralen-derivative crosslinker used for fixing RNA−RNA hybrids, for 15 minutes on ice and then lysed on ice. The homogenized lysate was hybridized with probes (mixture of probe Circ-CDYL1 and Circ-CDYL2) for 180 min. Following hybridization, the streptavidin-coated magnetic beads were resuspended in the lysate mixture and incubated at 37°C for 30 min with rotated mixing. Following incubation, RNA was eluted by resuspending the beads twice in 50 μL RAP Elution Buffer and incubating at 95°C for 2 min. Then, the eluate was collected. Finally, the eluate protein was collected, and Western blot assays were performed.

M^6A-RNA binding protein immunoprecipitation (meRIP) assay

MeRIP was performed using a Magna RIP RNA-binding protein immunoprecipitation kit (17–700, Millipore) and a Dynabeads kilobase BINDER kit (60101, Invitrogen) according to the manufacturers' instructions and previous study.[25] In brief, Dynabeads were incubated with anti-m^6A antibody (5 μg; Synaptic Systems, #202003) for 1 h at room temperature. Precleared cell lysates were incubated with antibody-conjugated beads for 1 h at 4°C. Beads were washed five times, and binding complexes were eluted and subjected to RT−qPCR assay as described above.

Ligase-dependent absolute quantification of the m^6A modification fraction at specific sites in RNAs

The ligase-dependent absolute quantification of m^6A modification was performed by Aksomics (Shanghai, China). In brief, total RNA isolated from the HCCLM3 cell line was pretreated with RNase R. RNA spikes (100 pM) were added to 1 μg RNA and mixed with 20 nM probe L, 20 nM probe R, and 1×T3 ligation buffer (NEB). Then, the samples were incubated at 85°C for 3 min and cooled to 35°C for 10 min. The sample and the standard were subjected to real-time PCR. The RNA content corrected for m^6A methylation of the target gene site for the sample= (Total cDNA concentration of target gene - cDNA concentration of target gene site not m^6A methylated) * RNA spike in RNA concentration/cDNA concentration concentration of RNA spike in.

MazF-dependent quantification of m^6A modification in RNAs

The MazF-qPCR m^6A modification assay was performed by Aksomics (Shanghai, China). In brief, total RNA isolated from the HCCLM3 cell line was pretreated with RNase R. Then, the RNA sample was divided into two equal parts, and MazF (20 U/μl) was added to one part for digestion. MazF-treated and untreated samples were simultaneously subjected to cDNA synthesis, followed by a qPCR assay. The relative m^6A modification level of the samples was calculated by $2^{-\Delta\Delta CT}$.

CCK8, spheroid formation, and colony formation assays

CCK8: HCC cells were seeded in 96-well plates at a density of 2×10^3 cells per well. The viability of HCC cells was determined by Cell Counting Kit 8 (Dojindo, Japan) and measured at OD450 nm with the BioTek Gen5 system (BioTeck, USA) at 0, 24, 48, 72, 96 hours after seeding.

Spheroid formation: HCC cells were seeded in 6-well low-adhesion plates at a density of 3×10^3 cells per well. After 2 weeks, spheroids were observed using ImageJ software (NIH Image).

Colony formation: HCC cells were seeded in 6-well plates at a density of 3×10^3 cells per well. After 2 weeks, spheroids were observed using ImageJ software (NIH Image).

Limiting dilution: Cells were seeded into 96-well ultralow attachment microplates (Corning) at doses from 500 to 5 (8 wells per dose) and incubated under spheroid conditions for 2 weeks. Based on the frequency of wells without colonies, the proportion of T-ICs was determined using Poisson distribution statistics and L-Calc Version 1.1 software (Stem Cell Technologies, Inc., Vancouver, Canada).

Lentiviral infection

The lentivirus for overexpression of Circ-CDYL, Circ-CDYL^{mut} and EpCAM-mCherry fusion was produced by GeneChem Company (Shanghai, China), and that for overexpression of METTL3 and YTHDC1 was produced by Heyuan Biotechnology (Shanghai, China). Lentiviral infection was carried out according to the manufacturers' instructions. HCCLM3 cells and SMMC-7721 cells were infected with the concentrated virus at a multiplicity of infection (MOI) of 20 in the presence of 8 μg/mL polybrene (Sigma) for 10 hours. The expression of Circ-CDYL in the infected cells was validated by qRT−PCR. Puromycin (1 ng/μl) was used to screen infected cells according to the manufacturers' instructions.

For the Circ-CDYL and Circ-CDYL^{mut} stable overexpression system, the "flank strategy" was used to form Circ-CDYL. Briefly, specific intron sequences at both ends of mature circRNAs were constructed, which could promote the formation of circles. The sequence (the capital letters) and the two ends of the loop arms (lowercase letters) needed to build the lentivirus are as follows.

Circ-CDYL

gccagaaatgtactgacgttcttaataattgataggtgcagacctttgcgttcttaattaaagagccactccgtggctgtaggcctctgcccacaagatacagagtcacatgctgcccccaggatg
caagctgatgcttttatagtaactgcagatgtaataacagattctaggtatttcttcagtaacgtatggaggcactgtgtcacataactctcgttcatgtgagtagcggaagatctctcttccatttacg
cttcagatgttaaggtagtagaatttgtcacggtgataaaacgtgcttacaaggcagggttgtgtgaattgataaatttgatccaaaatgtattggtcatccatttcaatgattaacagcatctccattg
aaagatgttagtgtaaaattaattaaaaccaagatttgaaaataacctgatcgctctagactgttttattacaatcaagtatgatgttctctgttgacctttttagttttaattgagtgcttctgaatgatacttg
tgatacagatcatatgtttctttgatggcagtttcacaccacagaaggttctcagcgccttgtagctcattgctgtcaccactccaggctgttgcctgggtgcccgctgctggaaccctgggatgacc
aggcacagctgcagatgcctcgagctgctccagccatgagtgtggaaaccaactcggtggtcaggcttcaacacagaaatagcagagagccccctttcagtcacaagaaacataagtcacctaa
tgcatatccacacgttctcagcataaaaatttagcatcttgtttgacttactttcagggaaattgtccacaacccaaatggcctattactattttattgaggttgcagaagagatcattttatcatctattgt
ggtttttgctatttttgatgtttcctaatgaaacttgcacttttccccccaaattttgatttttttaaaactatttttttccttttatgaacagGTTGAAAGGATTGTTGACAAAAGGAAAAATA
AAAAAGGGAAGACAGAGTATTTGGTTCGGTGGAAAGGCTATGACAGCGAGGACGACACTTGGGAGCCGGAACAGCACCTCGTGAACT
GTGAGGAATACATCCACGACTTCAACAGACGCCACACGGAGAAGCAGAAGGAGAGCACATTGACCAGAACAAACAGGACCTCTCCCA
ACAATGCTAGGAAACAAATCTCCAGATCCACCAACAGCAACTTTTCTAAGACCTCTCCTAAGGCACTCGTGATTGGGAAAGACCACGAA
TCCAAAAACAGCCAGCTGTTTGCTGCCAGCCAGAAGTTCAGGAAGAACACAGCTCCATCTCTCTCCAGCCGGAAGAACATGGACCTAG
CGAAGTCAGGTATCAAGATCCTCGTGCCTAAAAGCCCCGTTAAGAGCAGGACCGCAGTGGACGGCTTTCAGAGCGAGAGCCCTGAGA
AACTGGACCCCGTCGAGCAGGGTCAGGAGGACACAGTGGCACCCGAAGTGGCAGCGGAAAAGCCGGTCGGAGCTTTATTGGGCCCC
GGTGCCGAGAGGGCCAGGATGGGGAGCAGGCCCAGGATACACCCACTAGTGCCTCAGGTGCCCGGCCCTGTGACTGCAGCCATGGC
CACAGGCTTAGCTGTTAACGGGAAAGgtgagtgtctagggagctgctcaggctccgtggtgatcccagagggctcgggtccttctctagagatcaggccttgagctgggcag
agtccggggcttctcacggcatctgctggagccttgcagagatttcgccttctcctttcttcgctggaagcctttgatatttctcttaattcggcaactagttttttctgtgtaattcgccatccacagactg
tgctaccacactgacttgctttaaacagtatctccctctaactaggttattaggtgataagtttttacagcaagtttctgaagctgtctacctttcttcacctctgaagtgctgagtcttgtctcgtgttaag
cgttttcttctaagtgtggccagcattgatacagaagtgcaggttcttattttgctcatctgtgtgaatacccaggaatgcctttcagtgggagcgttgctaacccagcagagcctttgggagccgg
gctcgtttctctgttgtgatcggcagtgcaggtgccattgcttcccccgtcagagcccagtctgcctggcaccggtggtgtcctctgttttactctcatccccagccccgctcctgggttc.

Circ-CDYL^{mut} (bold letters refer to the mutant sites)

gccagaaatgtactgacgttcttaataattgataggtgcagacctttgcgttcttaattaaagagccactccgtggctgtaggcctctgcccacaagatacagagtcacatgctgcccccaggatgc
aagctgatgcttttatagtaactgcagatgtaataacagattctaggtatttcttcagtaacgtatggaggcactgtgtcacataactctcgttcatgtgagtagcggaagatctctcttccatttacgct
tcagatgttaaggtagtagaatttgtcacggtgataaaacgtgcttacaaggcagggttgtgtgaattgataaatttgatccaaaatgtattggtcatccatttcaatgattaacagcatctccattga
aagatgttagtgtaaaattaattaaaaccaagatttgaaaataacctgatcgctctagactgttttattacaatcaagtatgatgttctctgttgacctttttagttttaattgagtgcttctgaatgatactt
gtgatacagatcatatgtttctttgatggcagtttcacaccacagaaggttctcagcgccttgtagctcattgctgtcaccactccaggctgttgcctgggtgcccgctgctggaaccctgggatga
ccaggcacagctgcagatgcctcgagctgctccagccatgagtgtggaaaccaactcggtggtcaggcttcaacacagaaatagcagagagccccctttcagtcacaagaaacataagtcacc
taatgcatatccacacgttctcagcataaaaatttagcatcttgtttgacttactttcagggaaattgtccacaacccaaatggcctattactattttattgaggttgcagaagagatcattttatcatctat
tgtggtttttgctatttttgatgtttcctaatgaaacttgcacttttccccccaaattttgatttttttaaaactatttttttccttttatgaacagGTTGAAAGGATTGTTGACAAAAGGAAAAA
TAAAAAAGGGAAGACAGAGTATTTGGTTCGGTGGAAAGGCTATGACAGCGAGGACGACACTTGGGAGCCGGAACAGCACCTCGTGAT
CTGTGAGGAATACATCCACGACTTCAACAGACGCCACACGGAGAAGCAGAAGGAGAGCACATTGACCAGAACAAACAGGACCTCTCC
CAACAATGCTAGGAAACAAATCTCCAGATCCACCAACAGCAACTTTTCTAAGACCTCTCCTAAGGCACTCGTGATTGGGAAAGACCACG
AATCCAAAAACAGCCAGCTGTTTGCTGCCAGCCAGAAGTTCAGGAAGAACACAGCTCCATCTCTCTCCAGCCGGAAGATCATGGACCTA
GCGAAGTCAGGTATCAAGATCCTCGTGCCTAAAAGCCCCGTTAAGAGCAGGTCCGCAGTGGACGGCTTTCAGAGCGAGAGCCCTGAG
AATCTGGTCCCCGTCGAGCAGGGTCAGGAGGTCACAGTGGCACCCGAAGTGGCAGCGGAAAAGCCGGTCGGAGCTTTATTGGGCCCC
GGTGCCGAGAGGGCCAGGATGGGGAGCAGGCCCAGGATACACCCACTAGTGCCTCAGGTGCCCGGCCCTGTGTCTGCAGCCATGGC
CACAGGCTTAGCTGTTAACGGGAAAGgtgagtgtctagggagctgctcaggctccgtggtgatcccagagggctcgggtccttctctagagatcaggccttgagctgggcag
agtccggggcttctcacggcatctgctggagccttgcagagatttcgccttctcctttcttcgctggaagcctttgatatttctcttaattcggcaactagttttttctgtgtaattcgccatccacagact
gtgctaccacactgacttgctttaaacagtatctccctctaactaggttattaggtgataagtttttacagcaagtttctgaagctgtctacctttcttcacctctgaagtgctgagtcttgtctcgtgttaa
gcgttttcttctaagtgtggccagcattgatacagaagtgcaggttcttattttgctcatctgtgtgaatacccaggaatgcctttcagtgggagcgttgctaacccagcagagcctttgggagccg
ggctcgtttctctgttgtgatcggcagtgcaggtgccattgcttcccccgtcagagcccagtctgcctggcaccggtggtgtcctctgttttactctcatccccagccccgctcctgggttc.

For the EpCAM-mCherry fusion, METTL3, and YTHDC1 stable overexpression system, the sequence of gene of interest to build the lentivirus was as follows.

EpCAM-mCherry fusion

AGGTGTCCACTCCCAGGTCCAACTGCACCTCGGTTCTAAGCTTCTGCAGGTCGACTCTAGAGGATCCCGCCACCATGGCGCCCCCGCA
GGTCCTCGCGTTCGGGCTTCTGCTTGCCGCGGCGACGGCGACTTTTGCCGCAGCTCAGGAAGAATGTGTCTGTGAAAACTACAAGCTG
GCCGTAAACTGCTTTGTGAATAATAATCGTCAATGCCAGTGTACTTCAGTTGGTGCACAAAATACTGTCATTTGCTCAAAGCTGGCTGCCA
AATGTTTGGTGATGAAGGCAGAAATGAATGGCTCAAAACTTGGGAGAAGAGCAAAACCTGAAGGGGCCCTCCAGAACAATGATGGGCT
TTATGATCCTGACTGCGATGAGAGCGGGCTCTTTAAGGCCAAGCAGTGCAACGGCACCTCCATGTGCTGGTGTGTGAACACTGCTGGG
GTCAGAAGAACAGACAAGGACACTGAAATAACCTGCTCTGAGCGAGTGAGAACCTACTGGATCATCATTGAACTAAAACACAAAGCAAG
AGAAAAACCTTATGATAGTAAAAGTTTGCGGACTGCACTTCAGAAGGAGATCACAACGCGTTATCAACTGGATCCAAAATTTATCACGAG
TATTTTGTATGAGAATAATGTTATCACTATTGATCTGGTTCAAAATTCTTCTCAAAAAACTCAGAATGATGTGGACATAGCTGATGTGGCTT
ATTATTTTGAAAAAGATGTTAAAGGTGAATCCTTGTTTCATTCTAAGAAAATGGACCTGACAGTAAATGGGGAACAACTGGATCTGGATCC
TGGTCAAACTTTAATTTATTATGTTGATGAAAAAGCACCTGAATTCTCAATGCAGGGTCTAAAAGCTGGTGTTATTGCTGTTATTGTGGTTG
TGGTGATAGCAGTTGTTGCTGGAATTGTTGTGCTGGTTATTTCCAGAAAGAAGAGAATGGCAAAGTATGAGAAGGCTGAGATAAAGGAG
ATGGGTGAGATGCATAGGGAACTCAATGCAGGAGGTGGAGGATCAATGGTGAGCAAGGGCGAGGAGGATAACATGGCCATCATCAAG
GAGTTCATGCGCTTCAAGGTGCACATGGAGGGCTCCGTGAACGGCCACGAGTTCGAGATCGAGGGCGAGGGCGAGGGCCGCCCCTA
CGAGGGCACCCAGACCGCCAAGCTGAAGGTGACCAAGGGTGGCCCCCTGCCCTTCGCCTGGGACATCCTGTCCCCTCAGTTCATGTAC
GGCTCCAAGGCCTACGTGAAGCACCCCGCCGACATCCCCGACTACTTGAAGCTGTCCTTCCCCGAGGGCTTCAAGTGGGAGCGCGTG
ATGAACTTCGAGGACGGCGGCGTGGTGACCGTGACCCAGGACTCCTCCCTGCAGGACGGCGAGTTCATCTACAAGGTGAAGCTGCGC
GGCACCAACTTCCCCTCCGACGGCCCCGTAATGCAGAAGAAGACCATGGGCTGGGAGGCCTCCTCCGAGCGGATGTACCCCGAGGAC
GGCGCCCTGAAGGGCGAGATCAAGCAGAGGCTGAAGCTGAAGGACGGCGGCCACTACGACGCTGAGGTCAAGACCACCTACAAGGC
CAAGAAGCCCGTGCAGCTGCCCGGCGCCTACAACGTCAACATCAAGTTGGACATCACCTCCCACAACGAGGACTACACCATCGTGGAA
CAGTACGAACGCGCCGAGGGCCGCCACTCCACCGGCGGCATGGACGAGCTGTACAAGTAACTCGAGTCCATCGATACTAGTCTGTGGA
ATGTGTGTCAGTTAGGGTGTGGAAAGTCCCCAGGCTCCCCAGCAGGCAGAAGTATGCAAAGCATGCATCTCAATTAGTCAGCAACCAG
GTGTGGAAAGTCCCCAGGCTCCCCAGCAGGCAGAAGTATGCAAAGCATGCATCTCAATTAGTCAGCAACCATAGTCCCGCCCCTAACT
CCGCCCATCCCGCCCCTAACTCCGCCCAGTTCCGCCCATTCTCCGCCCCATGGCTGACTAATTTTTTTTATTTATGCAGAGGCCGAGGCC
GCCTCTGCCTCTGAGCTATTCCAGAAGTAGTGAGGAGGCTTTTTTGGAGGCCTAGGCTTTTGCAAAAAGCTCCCGGGAGCTTGTATATCC
ATTTTCGGATCTGATCGCCACCATGACCGAGTACAAGCCCACGGTGCGC.

METTL3

ATGTCGGACACGTGGAGCTCTATCCAGGCCCACAAGAAGCAGCTGGACTCTCTGCGGGAGAGGCTGCAGCGGAGGCGGAAGCAGGA
CTCGGGGCACTTGGATCTACGGAATCCAGAGGCAGCATTGTCTCCAACCTTCCGTAGTGACAGCCCAGTGCCTACTGCACCCACCTCTG
GTGGCCCTAAGCCCAGCACAGCTTCAGCAGTTCCTGAATTAGCTACAGATCCTGAGTTAGAGAAGAAGTTGCTACACCACCTCTCTGAT
CTGGCCTTAACATTGCCCACTGATGCTGTGTCCATCTGTCTTGCCATCTCCACGCCAGATGCTCCTGCCACTCAAGATGGGGTAGAAAGC
CTCCTGCAGAAGTTTGCAGCTCAGGAGTTGATTGAGGTAAAGCGAGGTCTCCTACAAGATGATGCACATCCTACTCTTGTAACCTATGCT
GACCATTCCAAGCTCTCTGCCATGATGGGTGCTGTGGCAGAAAAGAAGGGCCCTGGGGAGGTAGCAGGGACTGTCACAGGGCAGAAG
CGGCGTGCAGAACAGGACTCGACTACAGTAGCTGCCTTTGCCAGTTCGTTAGTCTCTGGTCTGAACTCTTCAGCATCGGAACCAGCAAA
GGAGCCAGCCAAGAAATCAAGGAAACATGCTGCCTCAGATGTTGATCTGGAGATAGAGAGCCTTCTGAACCAACAGTCCACTAAGGAA
CAACAGAGCAAGAAGGTCAGTCAGGAGATCCTAGAGCTATTAAATACTACAACAGCCAAGGAACAATCCATTGTTGAAAAATTTCGCTC
TCGAGGTCGGGCCCAAGTGCAAGAATTCTGTGACTATGGAACCAAGGAGGAGTGCATGAAAGCCAGTGATGCTGATCGACCCTGTCGC
AAGCTGCACTTCAGACGAATTATCAATAAACACACTGATGAGTCTTTAGGTGACTGCTCTTTCCTTAATACATGTTTCCACATGGATACCTG
CAAGTATGTTCACTATGAAATTGATGCTTGCATGGATTCTGAGGCCCCTGGCAGCAAAGACCACACGCCAAGCCAGGAGCTTGCTCTTAC
ACAGAGTGTCGGAGGTGATTCCAGTGCAGACCGACTCTTCCCACCTCAGTGGATCTGTTGTGATATCCGCTACCTGGACGTCAGTATCTT
GGGCAAGTTTGCAGTTGTGATGGCTGACCCACCCTGGGATATTCACATGGAACTGCCCTATGGGACCCTGACAGATGATGAGATGCGC
AGGCTCAACATACCCGTACTACAGGATGATGGCTTTCTCTTCCTCTGGGTCACAGGCAGGGCCATGGAGTTGGGGAGAGAATGTCTAAA
CCTCTGGGGGTATGAACGGGTAGATGAAATTATTTGGGTGAAGACAAATCAACTGCAACGCATCATTCGGACAGGCCGTACAGGTCAC
TGGTTGAACCATGGGAAGGAACACTGCTTGGTTGGTGTCAAAGGAAATCCCCAAGGCTTCAACCAGGGTCTGGATTGTGATGTGATCGT
AGCTGAGGTTCGTTCCACCAGTCATAAACCAGATGAAATCTATGGCATGATTGAAAGACTATCTCCTGGCACTCGCAAGATTGAGTTATT
TGGACGACCACACAATGTGCAACCCAACTGGATCACCCTTGGAAACCAACTGGATGGGATCCACCTACTAGACCCAGATGTGGTTGCA
CGGTTCAAGCAAAGGTACCCAGATGGTATCATCTCTAAACCTAAGAATTTATAG.

YTHDC1

ATGGCGGCTGACAGTCGGGAGGAGAAAGATGGAGAACTTAATGTTCTGGATGATATTTTAACTGAAGTACCAGAACAAGATGATGAACT
GTATAATCCAGAGAGTGAACAAGATAAAAATGAGAAAAAGGGATCAAAAAGAAAAAGTGATCGAATGGAATCTACTGATACCAAACGAC
AAAAGCCTTCTGTCCATTCTAGACAACTGGTTTCTAAGCCACTGAGCTCATCTGTTAGCAATAACAAAAGAATAGTTAGTACAAAAGGAAA
GTCAGCCACAGAGTATAAAAATGAGGAATATCAAAGATCTGAAAGAAACAAGCGTCTAGATGCTGATCGGAAAATTCGTCTATCAAGTAG

TGCCTCCAGAGAACCTTATAAGAATCAACCTGAAAAAACCTGTGTCCGGAAAAGGGATCCTGAAAGGAGGGCCAAATCTCCTACGCCA
GATGGTTCTGAGAGAATTGGGCTTGAAGTGGATAGACGTGCAAGCAGATCCAGCCAGTCTTCTAAGGAAGAAGTGAACTCTGAAGAAT
ATGGCTCTGACCATGAGACTGGCAGCAGTGGTTCTTCTGATGAGCAAGGGAACAACACTGAGAATGAGGAGGAAGGAGTGGAAGAAG
ATGTGGAGGAAGATGAAGAAGTAGAAGAAGATGCAGAAGAAGATGAAGAGGTGGATGAAGATGGAGAGGAGGAGGAGGAAGAGGAG
GAGGAGGAAGAGGAGGAGGAGGAGGAGGAAGAAGAAGAATATGAACAGGATGAGAGAGACCAGAAAGAGGAGGGAAATGATTATG
ACACTCGAAGTGAGGCCAGTGACTCTGGTTCTGAATCTGTTTCCTTCACAGATGGGTCTGTCAGATCTGGTTCAGGCACAGATGGATCAG
ATGAGAAAAAGAAGGAAAGGAAGAGAGCTAGAGGCATATCTCCAATTGTTTTTGATAGAAGTGGAAGCTCTGCATCAGAGTCATATGCA
GGTTCAGAAAAGAAGCATGAGAAATTATCATCTTCCGTTCGTGCTGTCCGAAAAGATCAAACCAGTAAACTCAAATATGTGCTTCAAGAT
GCAAGATTTTTCCTCATAAAGAGTAACAACCATGAGAATGTGTCTCTTGCCAAAGCGAAGGGTGTATGGTCCACGCTCCCTGTAAATGAG
AAGAAATTAAATCTTGCATTTAGATCTGCAAGGAGTGTTATCTTAATATTTTCTGTCAGAGAGAGTGGAAAATTTCAAGGGTTTGCAAGAC
TTTCTTCAGAATCACATCACGGAGGATCTCCTATACACTGGGTGCTTCCAGCAGGAATGAGTGCTAAAATGCTGGGAGGTGTCTTTAAAA
TTGACTGGATTTGCAGGCGTGAATTACCCTTCACTAAGTCGGCTCATCTCACCAATCCTTGGAATGAACATAAACCAGTAAAGATCGGAC
GTGATGGACAGGAAATTGAACTTGAATGTGGAACCCAGCTTTGTCTTCTGTTTCCCCCCGATGAAAGTATTGACTTGTATCAGGTCATTCA
TAAAATGCGTCACAAGAGAAGAATGCATTCTCAGCCCCGATCACGAGGACGTCCATCCCGTCGAGAACCAGTCCGGGATGTGGGAAGG
CGTCGACCAGAAGATTATGATATTCATAACAGCAGAAAGAAACCAAGGATTGACTATCCCCCTGAGTTTCACCAGAGACCAGGGTATTTA
AAGGATCCACGATACCAGGAAGTGGACAGACGATTTTCAGGAGTTCGCCGAGATGTGTTTTTAAATGGGTCCTACAATGATTATGTGAGG
GAATTTCATAACATGGGACCACCACCACCTTGGCAAGGAATGCCCCCTTACCCAGGAATGGAACAACCTCCACACCATCCTTACTATCA
GCACCATGCTCCACCTCCTCAAGCTCATCCCCCTTACTCAGGACATCATCCAGTACCACATGAAGCAAGATACAGAGATAAACGAGTAC
ATGATTATGATATGAGGGTGGATGATTTCCTTCGTCGCACACAAGCTGTTGTCAGTGGCCGGAGAAGTAGACCCCGTGAAAGAGACCGG
GAACGAGAGCGAGACCGCCCTAGAGATAACAGACGAGACAGAGAGCGAGATAGAGGACGTGATAGAGAAAGAGAAAGAGAGCGATT
ATGTGATCGAGACAGAGACCGAGGGGAGAGAGGTCGATATAGAAGA.

siRNA transfection

The siRNAs for YTHDC1 and hnRNPA2B1 were purchased from Biotend Co. (Shanghai, China). Transfection was performed with JetPRIME reagents (Poly plus, Illkirch, France) according to the manufacturers' instructions. Briefly, $2*10^5$ cells were seeded into 6-well plates 24 hours before transfection. For each well, 10 μl (20 μM storage concentration) siRNA was added to the JetPRIME buffer. Mix by pipetting up and down. Then, JetPRIME was added to the siRNA duplexes and homogenized by vortexing immediately for 1 second. Incubate for 10 minutes at room temperature to allow transfection complexes to form between duplexes and JetPRIME. Then, the transfection mix was added to 2 ml of cell culture medium to a final concentration of 100 nM siRNAs. Finally, homogenize by gently swirling the plate.

Exosomes purification

The exosomes were purified using ultracentrifuge according to previous study.[50]

For cell-derived exosomes purification, cell lines were cultured in DMEM containing 10% exosomes-depleted FBS. After 48 h of culture, the cell culture medium was collected, and centrifuge through the following step: (1) Centrifuge 10 min at 300 × g, 4°C. Discard the pellet. (2) Centrifuge 20 min at 2,000 × g, 4°C. Discard the pellet. (3) Centrifuge 30 min at 12,000 × g, 4°C. Discard the pellet. Filter the suspension through a 0.22-μm filter. (4) Centrifuge 90 min at 120,000 × g, 4°C. Discard the supernatant. (5) Resuspend the pellet with 1 mL PBS. Centrifuge 70 min at 120,000 × g, 4°C. Discard the supernatant and collect the exosomes pellet.

For plasma-derived exosomes purification, 3 mL of venous whole blood samples of patients were collected using an anticoagulation tube (containing EDTA) (GD050EK2, Gongdong). The blood sample were centrifuged 10 min at 1,500 × g, 4°C, to collect 1 mL of plasma, and centrifuge through the following step: (1) Dilute plasma with triple volume of PBS, centrifuge 30 min at 2,000 × g, 4°C. Discard the pellet. (2) Centrifuge 45 min at 12,000 × g, 4°C. Discard the pellet. Filter the suspension through a 0.22-μm filter. (3) Centrifuge 90 min at 120,000 × g, 4°C. Discard the supernatant. (4) Resuspend the pellet with 1 mL PBS. Centrifuge 70 min at 120,000 × g, 4°C. Discard the supernatant and collect the exosomes pellet.

Exosomes identification

The identification of exosomes was performed by Echobiotech (Beijing, China). Exosomes were isolated from the cell culture supernatant of HCCLM3 and SMMC-7721 cells using ultracentrifugation. Exosomes were examined and photographed by electron microscopy using negative staining. Exosomes markers were detected using Western blot assays. The size of the exosomes was tested with a ZETASIZER Nano series-Nano-ZS (Malvern, England).

Flow cytometry analysis of exosomes

Flow cytometry was used to analyze the exosomes phenotype derived from cultured HCC cell or HCC patient plasma. Exosomes purified from cell supernatant or HCC patient plasma were coincubated with biotin-labeled anti-CD63 mAb (353018, Biolegend, San Diego, CA). Next, streptavidin beads were added and incubated for 2 h at RT. The bead/anti-CD63Ab/exosomes complexes were then coincubated with the fluorescein-conjugated monoclonal antibodies anti-EpCAM APC (369810, Biolegend, San Diego, CA) or with the isotype control (400222, Biolegend, San Diego, CA) at 4°C in the dark overnight. The samples were analyzed using a Beckman MoFlo XDP™ flow cytometer

(Beckman Coulter, USA). The analysis of the raw exosomes flow cytometry data was performed according to a previous study.[51] The positive gate was set at the point where <2% of the isotype control was positive. The results are presented as relative fluorescence values (%).

For LTi-Exos and NLTi-Exos subpopulation sorting, the final volume of samples was increased to 1 ml using 0.5% BSA in PBS before sorting. The samples were analyzed using a Beckman MoFlo XDP™ flow cytometer (Beckman Coulter) and sorted using a Beckman MoFlo XDP™ flow cytometer smart sampler (Beckman Coulter).

Exosomal RNA isolation and PCR analysis

Exosomal total RNA was isolated from cell- or plasma-derived exosomes using the exoEasy Maxi Kit (76064, Qiagen) following the manufacturer's instructions. The total amount of RNA for each reverse transcription reaction was 100 ng, and the complementary DNA template was prepared using an iScript™ cDNA Synthesis Kit (1708891, Bio-Rad) according to the manufacturer's protocol. The complementary DNA was amplified in a reaction mix of SYBR Green (Takara) using a LightCycler® 96 Real-Time PCR System (Roche) according to the manufacturer's instructions.

Exosomes labeling

Purified exosomes from HCC cell line supernatants were labeled using the red fluorescent lipid dye PKH26 kit (Wayenbio, ESQ-R-001) following the manufacturer's instruction, and then incubated with SMMC-7721 cells at 37°C for 12 hours. The cocultured cells were then fixed and labeled using Actin-Tracker Green (Beyotime, C1033) following the manufacturer's instruction.

STM2457 treatment

For *in vitro* treatment, HCC cell lines were treated with STM2457 at a final concentration of 5 μM or DMSO (1:1000 v/v) for 48 h. For *in vivo* treatment, xenografted nude mice were given intraperitoneal injections of 50 mg/kg STM2457 or vehicle every day.

Flow cytometry analysis of cells

Cells were collected and incubated for 30 min with 1% bovine serum albumin (BSA, Gibco) in PBS to block nonspecific antigens. Conjugated antibody (EpCAM-APC: 369810; CD133-APC, 397906; CD24-APC, 382604, Biolegend) incubation for cells was performed at 4°C for 10 minutes. The samples were analyzed using a Beckman MoFlo XDP™ flow cytometer (Beckman Coulter).

Western blot

Cell lysates were prepared with lysis buffer (Beyotime Biotechnology, China) and centrifuged at 12,000 × g for 20 min to collect the supernatant. Protein concentrations were determined using the bicinchoninic acid (BCA) assay. Immunoblotting was performed using specific primary antibodies as shown in key resources table. Immunocomplexes were incubated with the fluorescein-conjugated secondary antibody and then detected using an Odyssey fluorescence scanner (Li-Cor, Lincoln, NE).

Actinomycin D treatment

HCC cells were plated into six-well plates. After 4 h, cells were treated with actinomycin D (5 μg/mL) or DMSO (1:1000 v/v), and collected after 0, 1, 4, 8, and 12 hours of treatment.

RNA isolation and PCR analysis

Total RNA was isolated from cells using TRIzol Reagent (Invitrogen, USA) following the manufacturer's instructions. The complementary DNA template was prepared using oligo (dT) random primers and Moloney murine leukemia virus reverse transcriptase (Promega, USA) according to the manufacturer's protocol. After reverse transcription, the complementary DNA template was quantitated using real-time PCR technology. The primers used in this study were designed using the Primer-BLAST tool provided by www.ncbi.nlm.nih.gov. cDNA was amplified in a reaction mix of SYBR Green (Takara, Japan) with a LightCycler 96 Real-Time PCR System (Roche, Basel, Switzerland) according to the manufacturer's instructions. The mRNA levels were normalized against β-actin in cell and tissue lysates. Real-time PCR experiments for each gene were performed on 3 separate occasions.

QUANTIFICATION AND STATISTICAL ANALYSIS

All statistical analyses were performed with SPSS 18.0 software. Qualitative variables were analyzed by the chi-square test or Fisher's exact test. For continuous variables that obey the normal distribution, Student's *t* test was used to compare the differences. Otherwise, variables with an abnormal distribution were compared using a nonparametric test. Differences between groups were compared using analysis of variance (ANOVA) when applicable or a nonparametric test. Correlation analysis was performed using the Pearson correlation coefficient method. Unless otherwise specified, the results are presented as the means ± standard deviations (SD). All statistical tests were 2 sided, and $p < 0.05$ was considered statistically significant. In each graph, otherwise specifically mentioned, *$p < 0.05$, **$p < 0.01$, ***$p < 0.001$. NS stands for "not significant".